Metal Phosphides and Sulfides in Heterogeneous Catalysis: Electronic and Geometric Effects

Yanan Liu[a], Alan J. McCue[b*] and Dianqing Li[a*]

[a] *State Key Laboratory of Chemical Engineering, Beijing University of Chemical Technology, Beijing 100029, China.*

[b] *Department of Chemistry, University of Aberdeen, Aberdeen AB24 3UE, UK*

* Corresponding author

Tel: +44 1224 272915

E-mail address: a.mccue@abdn.ac.uk (Alan McCue); lidq@mail.buct.edu.cn (Dianqing Li)

ABSTRACT:

The efficiency of a heterogeneous catalyst depends on the nature and the number of catalytically active sites but these are often inhomogeneous. One possible solution is to construct site-isolated catalysts in which most, if not all, of the sites are structurally uniform and well-defined. Metal phosphides and sulfides form with distinct crystal structures based on a range of component stoichiometries. Hence, incorporating active components (i.e., the catalytically active metal) into this structure can regulate geometric arrangements in a more reproducible manner where non-metal atoms act as spacers around metal atoms to create isolated sites. A d-metal/p-block element strategy can provide several advantages compared with other methods which generate discrete active sites, including convenient synthesis, good process economics and improved catalyst stability. Interestingly, the metal atoms in these systems still show typical catalyst traits associated with the metal which opens up many possible catalytic applications. This review presents several interesting synthesis methods for preparing metal phosphides and sulfides and aims to draws links between geometric structure/electronic properties and enhanced catalytic performance (i.e., enhanced activity, selectivity and stability) for both petrochemical and fine chemical processes. With precise knowledge of metal phosphide and sulfide structures/active sites, we

envision the development of practically useful d-metal/p-block element catalysts from powder formulations to more industrial type pellets. It should, however, be noted that these materials are not without additional complexities. For example, metal phosphides and sulfides can have complex surface chemistry and operating environment can induce structural evolution. These factors also need to be carefully considered.

Keyword: Site isolation, d-metal/p-block elements, metal sulfides, metal phosphides, heterogeneous catalysis

1. Introduction to topic

Challenges in terms of energy and the environment create pressure on the scientific community to improve solutions through catalysis.[1] Owing to their robustness and operational practicality, heterogeneous catalysts are widely employed for a broad range of industrial process. However, these materials are far from perfect since they have finite turnover numbers, limited lifetimes and offer imperfect selectivity. These issues reflect the fact that heterogeneous catalysts, are highly complex materials which contain a variety of potential active sites. Recently, there has been great interest in creating site-isolated heterogeneous catalysts, where the active site does not form part of an extended structure (i.e., a continuous metal ensemble) but is instead geometrically separated in some manner.[2,3] The active site may still involve multiple metal atoms (i.e., dimers or trimers or larger clusters) or individual metal atoms. The latter eventuality represents the highest utilization efficiency of the active metal and may be referred to as 'single-atom catalysis'. Site isolation changes the appearance of a catalyst to an adsorbate such that it appears more like a series of independent active sites and this can be beneficial (Fig. 1). For example, site-isolated metal atoms can create low-coordinate environments and increase surface free energy,[4,5] promoting chemical interactions with the adsorbates.[6,7] However, many industrial processes rely upon supported metal catalysts where the active sites are inherently less well defined. For example, a multitude of sites such as steps, edges and terraces exist with the relative proportions of these changing with particle size (and composition for a bimetallic system).[8,9]

Researchers are thus interested in establishing ways of making supported metal type catalysts more uniform, whilst also having the ability to control active site geometry.

Much effort have been dedicated to achieving site-isolation by maximizing interactions between the metal atoms or supports.[10] Although a mass-selected soft-landing method is useful for preparing single-atom catalysts (and powerful for fundamental studies), low-yields and high expense limits application in practice.[11] Therefore, wet chemical techniques are often used to fix isolated metal atoms on the support surface since metal precursors already contain the metal dispersed on an atomic level.[12,13] A few studies have anchored metal atoms to defect sites of a support surface[14,15] or ion-exchanged metals supported on zeolites.[16] This can help avoid agglomeration in post-treatment processes but is generally restricted to low metal loading (<1 wt.%) and may result in an uneven distribution of the active metal sites which makes it difficult to reveal the catalytic mechanism.[17] Atoms like nitrogen and sulfur contain lone pairs of electrons which can coordinate metal atoms and serve as coordination sites to stabilize and isolate more metal atoms.[18] A spatial confinement strategy using porous materials like metal-organic frameworks is another promising approach to synthesize high metal loading site-isolated catalysts.[19] An alternative approach can involve combining a metal with a second metal element (alloying/intermetallic) to enhance metal isolation degree which could be more controllable, even with high metal loading.[20,21] For instance, by alloying Cu atoms with Pd by physical vapor deposition, Sykes et al. constructed single atom alloys (in which Pd sites are totally isolated) and found the isolated Pd atoms facilitated H_2 activation for selective hydrogenation.[22] However, the complexity of the fabrication route renders these techniques challenging for industry. It would therefore be desirable to find alternative methods to create site-isolated catalysts.

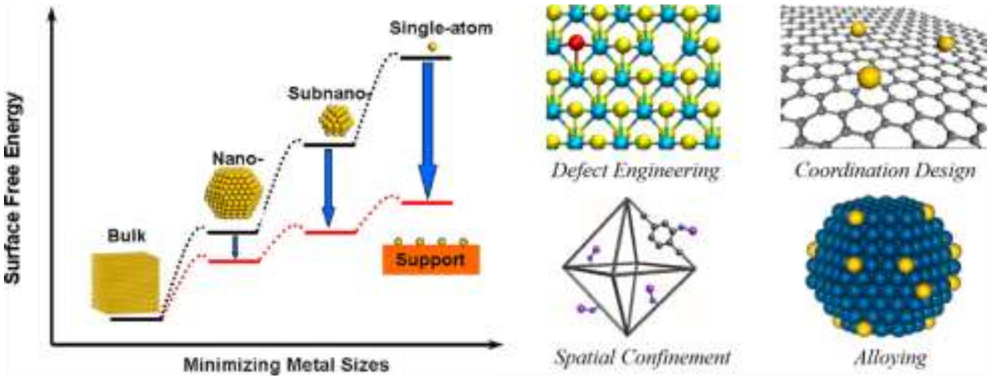

Fig.1 Left - Schematic diagram illustrating the change of surface free energy per metal atom with metal particle size with/without support. The black line represents the surface free energy state of metal particles at different scales, while the red line represents the energy state of the equivalent supported atom/particle. The blue arrow represents the process of loading active metal on to the support. Right - synthetic strategies for achieving isolated active metal atoms. Reproduced from ref 20. Copyright 2013 American Chemical Society.

Transition metal/p-block materials form with a range of transition metals (especially in the VIII group) and p-block elements (especially non-metal elements in the first two rows of p-block) with the most common being sulfides and phosphides.[23,24,25] In the 1970s, Sauer et al.[26] reported that metal-rich phosphides, showed excellent hydrogenation activity. More recently, synthetic developments since the late 1990's have generated a variety of d-metal/p-block materials with distinct crystal structures based on component stoichiometry (M_xN_y).[23, 27] Hence, incorporating active components into this structure can regulate geometric arrangements in a reproducible manner where non-metal atoms act as spacers around metal atoms to create isolated sites for heterogeneous catalysis. Interestingly, the metal atoms in these systems show typical traits associated with metal functionality (i.e., active/effective for hydrogenation/dehydrogenation). By varying the component ratio, researchers have an interesting method to modify active site geometry. There is also a potential electronic effect to explore by coupling a metal with a more electronegative p-block element and this has been shown to be beneficial for certain application (see later).

In this review, we present a detailed survey of the following topics: (1) How metal phosphides and sulfides represent a relatively simple way of creating uniform active sites in a heterogeneous catalyst; (2) How these uniform active sites can be considered as 'site isolated' by having p-block elements act largely as spacers around active metal atoms; (3) Applicability of these systems to chemical processes of specific importance for the petrochemical, fine chemical and energy sectors; (4) How to study such systems through the combined use of experimental and theoretical approaches; (5) Extending this methodology from powder formulations to more industrial type pellets.

2. Synthesis of metal phosphides and sulfides

The p-block elements, especially non-metal elements in the first two rows of p-block (i.e., S, P, B, C and N) react with a variety of transition metals (i.e., Fe, Co, Ni, Pd, Pt) to generate a multifarious class of chemical compounds, of which the most common are metal phosphides and sulfides. These compounds can be fabricated in various forms including bulk phase materials, supported form and even ultrathin two-dimensional nanostructures. In section 2.1, we focus on synthesis methods which are primarily aimed at preparing bulk phase compounds. For heterogeneous catalysis, it is obviously desirable to increase the surface area of the active phase and hence supported systems are generally preferred. Therefore, the synthesis of supported metal-P block compounds will be specifically described in section 2.2.

2.1 Synthesis of unsupported metal phosphides and sulfides

2.1.1 Metal phosphides

Interest in the preparation of metal phosphides from P precursors first spiked in the 1970's. Over the last 40 years, research into bulk phase metal phosphides continued, although with more emphasis on nano-scaled materials. In this section, an overview and discussion of the main synthetic techniques for the preparation of bulk phase metal phosphides is provided. This includes traditional synthesis from pure elements, reduction with phosphorus-containing compounds and the decomposition of organometallic precursors. The latter of which is considered as a faster and more tunable method for preparing bulk phase materials, although it is still generally efficient when preparing nano-scaled compounds.

2.1.1.1 Synthesis from the elements

Bulk phase metal phosphides can be fabricated via a traditional solid-state route by direct reaction of the elements, as described in the earliest studies (see Fig. 2A), such as Table 1 - Entry 1.[28,29] Using this method, many high purity metal phosphides can be routinely prepared on a large scale. However, high temperatures and long reaction times under vacuum or an inert atmosphere are necessary to work with pyrophoric P_4 and phosphine which thus creates a hazard and makes it a less attractive route. In recent decades, solution-based methods (i.e., solvothermal synthesis) have become more popular as they generally involve the use of softer reaction conditions and safer reactants. In addition, a solution-based strategy also offers greater control over dispersion and morphology of the metal phosphide which could be considered important for heterogeneous catalysis. The first example described here (Table 1 - Entry 2)[30], employed white phosphorus (P_4) as a reagent (often in large excess relative to the metal). White phosphorous is highly reactive and so dissolution in the reaction medium (i.e., water, ethylenediamine, ammonia etc.) can help to precisely control the metal to phosphorous stoichiometry. Carenco *et al.*[31] described a novel synthesis of Ni_2P at low temperature by using labile P ligands, such as phosphine oxides or alkylphosphines. This process is described by the "all-ripening" mechanism where the ligand solubilizes the metal precursor to create a species which can react with P_4. In principle, the reaction can also occur directly on the surface of a metal nanoparticle (i.e, surface reaction followed by P diffusion in the particle) and this is known as the "all-templating" mechanism (Fig. 2B).[32] The approach could also be generalized to other metals including Fe,[33] Rh[34] and Cu[35]. The more stable red P can be also used in place of white P_4 to obtain phosphides in high purity (Table 1 - Entries 3-7)[36,37,38,39,40,41,42].

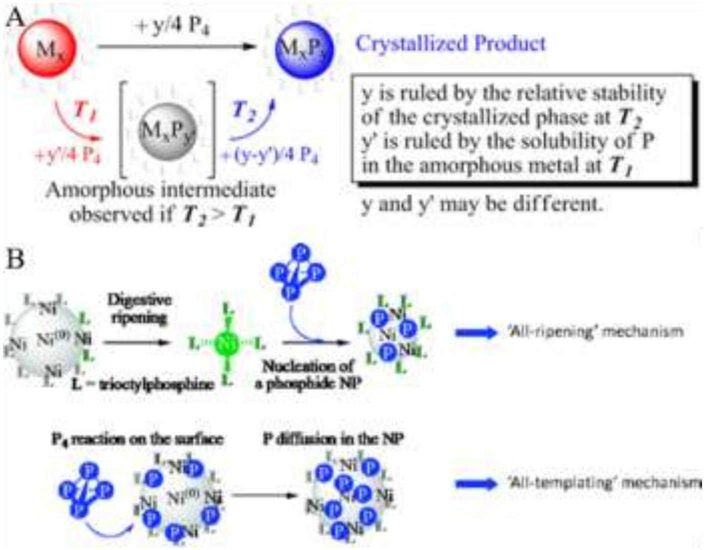

Fig. 2 (A) Schematic route from metal to metal phosphide nanoparticles via a traditional solid-state route by direct reaction of the elements. T is reaction temperatures. y is the relative amount of P observed at the end of the reaction in the crystalline nanoparticles, while y′ is the relative amount of P in the intermediate step. Several values for y are possible, and they depend on the metal, according to the M−P phase diagrams. Reproduced from ref 29. Copyright 2012 American Chemical Society. (B) Description of the two main pathways including "all-ripening" and "all-template" process for the conversion to NiP using white phosphorus as a "P" atom donor; Reproduced from ref 32. Copyright 2011 American Chemical Society.

2.1.1.2 Simple reduction of phosphates or hypophosphite

The phosphidation of metal precursors followed by temperature-programmed reduction of the resulting phosphate is a convenient strategy without expensive or harmful precursors. This approach became popular after the synthesis of unsupported MoP catalyst was first reported by Oyama et al. in 1998[27] and later.[43,44] Bimetallic formulations such as NiMoP samples have also been reported. Results revealed the surface composition of MoP can be changed within a narrow range (Mo:P = 0.90-1.10) but without altering the bulk phase composition.[45] The variation in surface composition has implications for catalytic applications and highlights the need for analysis by surface sensitive techniques in order to derive structure-performance relationships. The reduction step is often slow and requires elevated temperatures (400-1000ºC)[46,47,48,49] owing to the strong P=O bond in a phosphate.

Neither the use of high temperature nor the appearance of extraneous species contaminating the product are ideal, hence the development of a simple and green preparation process at low temperature is desirable. The simplest phosphating agent possible would be PH_3 although, it is toxic, potentially lethal and creates serious environmental concerns which mean direct phosphidation with this species is impractical. As a result, ammonia ($NH_4H_2PO_2$) or sodium (NaH_2PO_2) hypophosphites are far more common phosphorus sources since they are simpler to handle. When heating a hypophosphite to ca. 250°C, decomposition begins releasing PH_3 which can then react with the metal precursors to form a metal phosphide. According to this, some groups have explored low temperature preparation using hypophosphites, which could avoid sintering of the metal phosphide particles (Table 1 - Entry 9).[50,51] Furthermore, Miller et al.[52] employed sodium hypophosphite to generate PH_3 by thermal decomposition to convert metal oxides into a FeCo phosphide (metal oxides were obtained via a hydrothermal reaction between $Co(NO_3)_2 \cdot 6H_2O$ and $FeCl_3$). In this system, neither a surfactant nor a template was necessary which represents a cost saving. Also, low synthesis temperature is advantageous when targeting the controlled construction of defined nanocrystals.

2.1.1.3 Decomposition of organophosphorus compounds

Aside from controlled morphology of phosphide materials, the need for high-surface-area is pivotal for catalytic applications. Driven by this need, thermal decomposition of organometallic compounds or reaction with organophosphine reagents have been explored (Table 1 - Entries 10-12).[53,54,55,56] In these cases, trioctylphosphine oxide (TOPO) acts as a high boiling point solvent and a capping agent/ligand which inhibits agglomeration of the nanoparticles, but is not thought to act as the P source.[57,58] Tri-n-octylphosphine (TOP) is a less expensive and less toxic compound than $P(SiMe_3)_3$ and upon heating to ca. 300°C the C-P covalent bonds break to generate free phosphorus which can react with metal precursors to form a metal phosphide (Table 1 - Entries 13-14).[59,60] NiP nanoparticles can be derived from Ni^{2+} compounds like nickel acetylacetonate using TOP as a source of phosphorus and oleylamine as a reducing agent. The preparation process on both metal nanoparticles and model surface is shown in Fig. 3A and B.[61] On account of the strong coordination effect, TOP can effectively promote the reaction and synthesize materials with anomalous structure (Table 1 - Entry 15).[62] A similar method could be extended to the preparation of bimetallic M–Sn phosphide nanoparticles (M = Ni, Co and Fe), but with a metal chloride and tributylphosphine (TBP) as opposed to an organometallic Ni precursor and TOP (Fig. 3C).[63] Other organic phosphines (e.g. triphenylphosphine[64] or aminophosphines[65]) can be used as P precursors, although in some cases carbon may be incorporated into the resulting structure which may or may not be desirable,[66] given that carbide formation can greatly alter catalytic performance. In other words, linking structure and catalytic performance becomes somewhat challenging.

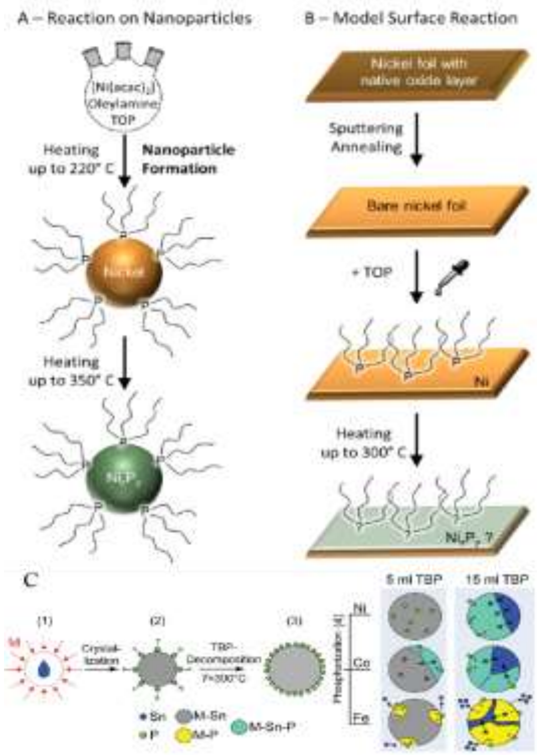

Fig.3 (A) Typical literature procedure for preparing Ni-P catalysts from tri-n-octylphosphine (TOP). (B) Surface processing steps to study insertion of phosphorus from TOP into Ni. Reproduced from ref 61. Copyright 2017 WILEY-VCH Verlag GmbH & Co. KGaA, Weinheim. (C) Proposed growth mechanism of M–Sn–P nanoparticles. (1) Formation of Sn-rich nanodroplets and further reaction with Sn- and M-monomers. (2) Intermetallic M–Sn nanoparticle stabilized by oleylamine and tributylphosphine (TBP). (3) Decomposition of TBP at 300ºC at the surface of the nanoparticle. (4) Diffusion of P into the nanoparticle and the resulting structures with different amounts of TBP. Reproduced from ref 63. Copyright 2019 Royal Society of Chemistry.

Table 1. Methodologies and precursors used to form bulk phosphides or sulfides

Entry	Material	Metal precursor	Source of P/S[a]	Method and reaction conditions
1	iron phosphorus[28]	Fe	red P	sealed evacuated silica tube followed by heating to 900°C for 8 days
2	Co_2P[30]	$CoCl_2\cdot 6H_2O$	white P	220°C for 24 h in aqueous ammonia
3	Cu_3P[36]	CuCl	red P	hydrothermal synthesis at 200°C
4	Ni_2P[37]	$NiCl_2$ hexahydrate	red P	a solvothermal process by heating at 180°C for 20 h.
5	Ni_5P_4[38]	metallic nickel powder	red P	reaction in an inert atmosphere at 500°C
6	ZrP[39, 40, 41]	$ZrCl_4$	Na_3P from white/red P	a solid-state metathesis at elevated temperature of 1000°C
7	orthorhombic Fe phosphide[42]	anhydrous $FeCl_3$	Na_3P	an equivalent route with benzene as solvent at 180-190°C
8	CoP[46]	$Co(NO_3)_2$	$(NH_4)_2HPO_4$	in-situ calcination at 500°C for 6 h and reduction in H_2 at 1000°C.
9	Ni or Fe phosphides[50,51]	$NiCl_2$ or α-Fe_2O_3	NaH_2PO_2	decomposition in a static protecting atmosphere at 300°C
10	MnP[53]	$Mn_2(CO)_{10}$	$P(SiMe_3)_3$	220°C
11	FeP[54]	$Fe(CO)_5$ or $Fe(acac)_3$	$P(SiMe_3)_3$	In TOPO at 270°C over 48 h
12	Ni_2P, $Ni_{12}P_5$[55,56]	$Ni(acac)_2$	TOP	320 °C; 300°C
13	InP[59]	$InCl_3$ with Na	TOP	at only 250°C
14	Cd_3P_2[60]	Cd	TOP	heated at 250 °C with stirring under inert atmosphere for about 10–12 h
15	NiP, CoP, FeP[62]	Oxides	TOP	dissolution reprecipitation method
16	MnS[71]	$MnCO_3$	H_2S	by annealing at 800°C
17	FeS[72]	Fe_2O_3	H_2S	the sulfidation at 200-300°C
18	Yolk-shell SnS[75]	SnO_2	H_2S	a spray pyrolysis route

[a] TOP = tri-n-octylphosphine

2.1.2 Metal sulfides

Although bulk phases require larger amounts of metals, synthesis of bulk metal sulfides has still progressed significantly over the past decades. In terms of nanostructured metal sulfides, there is interest in controlling composition and optimizing morphology and crystal structure. It is also useful to consider the role of quantum size effects in tuning electronic properties via changes to the valence band. In pursuit of these goals, preparation strategies have become diverse and include reaction in the gas phase or in organic solutions with/without template-assistance.

2.1.2.1 Treatment via inorganic sulfur compounds

The fabrication of active sulfide phases can involve the transformation of the metal or catalytically inactive oxide phase with inorganic sulfur compounds including gaseous H_2S or solid reagents. In the recent period, our group[67] prepared a crystalline Pd_4S phase from an amorphous PdS sample via H_2 reduction treatment (see Fig. 4A). Based on the phase diagram, palladium sulfide can form with a number of distinct compositions/structures (i.e., PdS, $Pd_{16}S_7$, Pd_3S and Pd_4S). Reduction of amorphous PdS at temperature of 150°C or higher resulted in the removal of a portion S from the sample (primarily as H_2S) to produce sulfur lean phases (i.e., $Pd_{16}S_7$ and Pd_4S). Depending on temperature, this treatment may result in a phase gradient across a particle since it relies on either diffusion of hydrogen into or sulfur out of the bulk. For example, reduction at 250°C generated a mixed core-shell structure with Pd_4S existing on the surface and $Pd_{16}S_7$ in the bulk, whereas treatment at 350°C resulted in a pure Pd_4S phase. Hollow metal sulfides such as FeS, CoS, MnS and Ag_2S were synthesized via the sulfidation of the Fe, Co and Mn oxides using sulfur powder or Na_2S.[68,69] It is also possible to prepare bimetallic sulfides from solid sulfur-containing compounds. For example, NiS_2/MoS_2 nanowires were synthesized by sulfiding a $NiMoO_4$ nanowire with S powder as source (Fig. 4B).[70] Whilst more research has focused on using solid state precursors, it is also possible to use H_2S as the sulfur source so long as the metal precursors are not vaporized during the fabrication (Table 1 - Entries 16-17).[71,72] CoS[73] and Co_9S_8,[74] acicular nanotube arrays (ANTAs) were prepared from cobalt oxide and $Co(CO_3)_{0.5}(OH)_x\cdot 11H_2O$ in an Na_2S solution. The influence of S source on the structure and morphology is an interesting phenomenon but with limited understanding to date. Out with the transition metals, it is also possible to form tin sulfides using H_2S (Table 1 - Entry 18).[75]

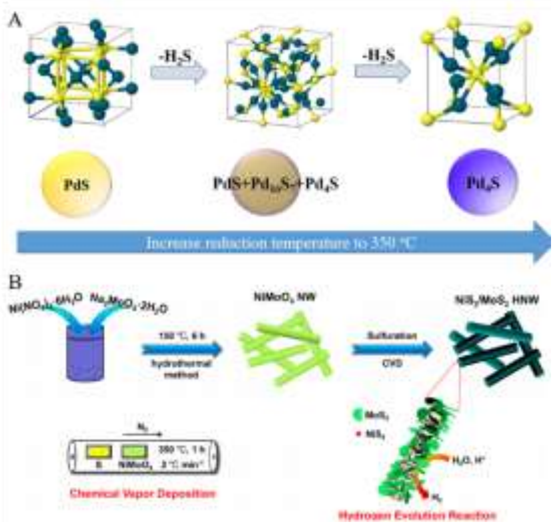

Fig. 4 (A) Conversion process from PdS to Pd_4S with increasing reduction temperature to 350°C. Reproduced from ref 67. Copyright 2018 Elsevier Inc. (B) Schematic illustration for the preparation of NiS_2/MoS_2. Reproduced from ref 70. Copyright 2017 American Chemical Society.

2.1.2.2 Solvo-thermal decomposition

A solvothermal route is similar to a hydrothermal method but uses an organic solvent as opposed to water. Dutta et al.[76] have attempted to develop a general solvothermal method to decompose the $[Fe_3(\mu_3\text{-}O)(\mu_2\text{-}O_2CCH_2Cl)_6(H_2O)_3]NO_3\cdot H_2O$ complex in the presence of thiourea as solvent at 150°C which lead to the growth of needle-like FeS structures. Ni doped $Zn_{0.5}Cd_{0.5}S$ could also be fabricated by this method using ethanol as the solvent, and $(NH_4)_2S$ as the vulcanizing agent.[77] Xu et al.[78] reported an interesting study where FeS nanosheets with a carbon coated surface (C@FeS) could be prepared via a simple surfactant-assisted technique where 1-dodecanethiol (DDT) acted as both surfactant and sulfur source. The procedure required reacting $Fe(acac)_3$ with an excess of DDT (Fe:DDT = 1:20) in oleylamine at 220°C before annealing at 400°C for 2 h in an Ar atmosphere. This approach is also suitable for a Cu-S system. For instance, ordered Cu_2S nanowire arrays have been successfully made where the diameter and length of Cu_2S nanowires were 40–120 nm and 700–1400 nm, respectively.[79] Cai et al.[80] reported a facile approach to prepare a mixed hexagonal CuS/Cu_2S nanotube. Here, synthesized Cu nanowires were treated with thiourea at 180–190°C in a solution of polyethylene glycol (PEG) under Ar by a solvothermal route. Interestingly, a mixed CuS/Cu_2S phase with ca. 32.3 wt% metallic Cu was obtained after the treatment for 30 min, whereas 120 min was required to form a pure sulfide, although both CuS and Cu_2S phases were observed.

2.2 Synthesis of supported metal phosphides and sulfides

Within the field of heterogeneous catalysis, supported materials are often required since this benefits from improved active phase dispersion. In this section we discuss the methods which can lead to well defined supported d-metal/p-block compounds (i.e., a single metal phosphide or sulfide phase as opposed to a mixture of phases since this is highly desirable for development of a structure-performance relationship). Similar to the synthesis of bulk d-metal/p-block compounds, traditional solid-state strategies such as reduction of p-block containing compounds and organometallic decomposition routes can be employed. For convenience, an overview of synthetic methodologies are presented in Table 2. It is important to acknowledge that the act of dispersing the active phase introduces an interfacial region between the metal phosphide/sulfide and the support material. This region may play a specific role in a catalytic reaction. Whilst this aspect is only considered fleetingly throughout this review it should not be dismissed out of hand.

Many researchers have sought to further optimize traditional solid-state strategies. For example, Ding et al.[81] developed a simpler and more efficient microwave heating route for the preparation of carbon supported Ni phosphides including Ni_5P_4, NiP_2 and Ni_2P phases. The synthesis involved the impregnation of $NiCl_2$ precursors onto an activated carbon, followed by milling with red P and subsequent microwave heating in a flow of H_2 or Ar at 160-200ºC for 10 min. Treatment in H_2 resulted in smaller particles (10-20 nm) than Ar. This was attributed to the conversion of red P to more active white P on microwave induced hot spots. This species could then react with H_2 to generate PH_3 leading to facile phosphination. Importantly, the presence of microwave irradiation enables synthesis at lower temperatures than conventional heating methods (Entries 1-3 in Table 2).[82,83,84]

As previously stated, phosphate reduction usually requires high temperatures to break the strong phosphate bond (Table 2 – entries 4-7)[85,86,87,88,89,90]. To overcome this issue, a sol–gel approach with the reduction of phosphates was used to synthesize SiO_2 supported Ni phosphides.[91] Ni/SiO_2 was first prepared by a sol–gel method before $NH_4H_2PO_4$ was then added via impregnation prior to calcination and reduction at 650°C - lower than that required by two-step reduction of phosphates (~800°C).[92,93] Despite 650°C still being a relatively high reduction temperature, this method can yield a single crystalline Ni_2P phase, which is crucial for the preparation of uniform isolated metal sites. Also, in this case, the sol–gel method contributed to a strong interaction of Ni with the support, which improved Ni dispersion and sintering resistance. These points are conducive for an effective and stable heterogeneous catalyst. When employing the phosphate route, one should note Al_2O_3 is not an ideal support since strong interactions can yield $AlPO_4$ instead of a metal phosphide.[94] To lower the treatment temperature, alternative precusors of phosphite or (hypo) phosphite have been extensively utilized for the construction of metal phosphides. A pioneering work of supported metal (Fe, Co, Ni, Ru, Mo, W, Rh, Pd, Pt) on alumina phosphides using phosphine (PH_3) as the phosphorus source were firstly reported by the group of Muetterties and Sauer,[26] followed by the preparation of NiP/SiO_2[95,96] using this kind of method. Moreover, Bui et al.[97] directly reacted phosphite with Ni, W, Mo, Co, Fe salts on SiO_2 to obtain a series of well-distributed and pure Ni_2P, WP, MoP, CoP and FeP nanocrystals (650-800°C necessary). Using this method, small particles can be formed even with active phase loading of up to 10 wt.%.[98] That coupled with a relatively simple synthesis should facilitate preparation of catalysts on a larger scale. But unfortunately, PH_3 was toxic and lethal although at very low concentration, leading to that it was not directly used however can be derived from hydrothermal $NH_4H_2PO_2$ or NaH_2PO_2 solution (Table 2 – entries 8-10).[99,100,101]

Organic phosphorus compounds can be used to prepare Al_2O_3 supported phosphide catalysts, which is advantageous since the reagents are more environmentally benign and well-defined stoichiometries can be prepared (Table 2 - Entries 11-13).[102,103,104] The specific interactions which lead to the formation of $AlPO_4$ are less significant with organometallic precursors which enables the use of Al_2O_3 as support. There are disadvantages to working with organometallic precursors though, such as the need work in the absence of oxygen and the combination of a hydrophobic precursor/solvent and hydrophilic support which makes impregnation into pores tougher. Interesting examples of this approach include the work of Liu and coworkers[105] who successfully synthesized CoP and Co_2P nanoparticles supported on CNTs via a facile thermal decomposition method from TOP. Bimetallic Pd−Ni−P nanoparticles on carbon support were fabricated from a mixture of $Pd(acac)_2$, $Ni(acac)_2$, tetrabutylammonium bromide (TBAB), oleylamine (OLA), with TPP as P source and TOPO as solvent.[106] As expected, this organic approach can be extended to the fabrication of supported metal borides.[107]

Supported metal sulfides can be prepared by conventional gas phase sulfidation and chemical vapor deposition (CVD) (Table 2 - Entries 14-18).[108,109,110,111,112] These techniques typically utilize H_2S or a vaporized S precursor to convert metal salts into sulfides but at relatively high temperature (~700–1000ºC). The temperature required can be lowered to 150-300ºC by using a plasma-enhanced CVD technique,[113,114] but the injection method is a challenge, since the axial mode can lead to plasma arc quenching, while the radial mode leads to uneven heating. Atomic layer deposition (ALD) is a subclass of the CVD technique in which films are grown by exposing the substrate surface to alternating precursors of gas molecules. Recently, ALD was used to grow a few-layers of metal sulfides on SiO_2/Si or Al_2O_3 substrate[115,116,117] using H_2S. The thickness could be controlled from a monolayer to few-layers for MS_2 (M = Mo/W) with tunable stoichiometry based on regulating the deposition time. The benefit of this method is an ability to produce materials with layer-by-layer precision. However, the deposition rate is relatively low, which makes it difficult to scale up. Not only the gas phase depositions have been utilized for the preparation of supported nanoscale metal sulfides, also employed the hydrothermal and solvothermal methods in the liquid phase (Table 2 - Entries 19-22),[118,119,120,121] in which the resource of non-metal element is still solid, but need to dissolved in the solution. A pure and highly dispersed Pd_4S phase was prepared on CNF support by impregnation with $PdSO_4$ followed by reduction in H_2 at 250°C.[122] The transformation of sulfate precursors in a sulfide was followed by high energy XRD analysis. For preparation of MoS_x,[123] N-doped carbon nanotubes (as the template) were immersed in an aqueous HCl solution containing $(NH_4)_2MoS_4$ before the precursor was decomposed at 90°C.

Table 2. Methodologies and precursors used to form supported phosphides or sulfides

Entry	Material	Metal precursor	Source of P/S	Method and reaction conditions
1	Ni_2P and FeP/Ni foam[82]	Ni foam or $Fe(NO_3)_3\cdot 9H_2O$,	P powder	chemical vapour deposition; 450°C in Ar atmosphere
2	FeP nanorods/C[83]	$FeCl_3\cdot 6H_2O$	red P	hydrothermal and gas-phase phosphidization reactions; 500°C
3	MoP/SiO_2[84]	$(NH_4)_6Mo_7O_{24}\cdot 4H_2O$	$NH_4H_2PO_4$	conventional heating method; 600°C
4	Ni_2P/SiO_2[85,86]	$Ni(NO_3)_2\cdot 6H_2O$	$(NH_4)_2HPO_4$	two-step programmed reduction of phosphates; 500-900°C
5	Ni_2P/SiO_2[87, 88]	$Ni(NO_3)_2\cdot 6H_2O$	$(NH_4)_2HPO_4$	reduction of phosphates; 350-600°C and passivated in 0.5% O_2/He
6	$NiMoP/SiO_2$[89]	$(NH_4)_6Mo_7O_{24}$ $Ni(NO_3)_2$	$(NH_4)_2HPO_4$	reduction of phosphates; 700°C and passivated in 1% O_2/He
7	carbon xerogels supported Fe_2P, Co_2P, $Ni_{12}P_5$[90]	metal nitrates	$(NH_4)_2HPO_4$	one-pot pyrolysis and carbothermal reduction; 800°C
8	Pd_3P/TiO_2 and PdP_2/TiO_2[99]	$PdCl_2$	$NH_4H_2PO_2$	reduction of hypophosphide; 500°C for 4 h in 20%H_2/N_2
9	Ru_2P/SiO_2[100]	$RuCl_3$	$NH_4H_2PO_2$	reduction of hypophosphide; 500°C and passivated in 1% O_2/He
10	NiP_2/C nanosheets[101]	$Ni(OH)_2$	NaH_2PO_2	two-step rout a hydrothermal route; 300°C
11	Ni_2P[102]	Ni foam	TOP	solvothermal method at 320°C
12	CoP/C[103]	cobalt(II) acetylacetonate	TOP	solvothermal method at 300°C
13	CoP/C core−shell[104]	cobalt(II) acetylacetonate	triphenylphosphine	heated in a sealed tube at 400°C for 100 min
14	MoS_2/Al_2O_3[108]	$(NH_4)_6Mo_7O_{24}\cdot 4H_2O$	H_2S/H_2	conventional gas phase sulfidation; at 100-450 °C
15	Pd_4S/C[109]	H_2PdCl_4	H_2S/H_2	conventional gas phase sulfidation; at 150-750 °C
16	$NiCo_2S_4$@CC[110]	$NiCl_2\cdot 6H_2O$ and $CoCl_2\cdot 6H_2O$	sulfur powder	annealing at 300°C
17	Mn_3S/C Nanowires[111]	$MnCl_2$	H_2S	chemical vapour deposition; at 673-1123 K
18	CoS/S-doped GO[112]	$Co(TU)_4(NO_3)_2$ complex	$Co(TU)_4(NO_3)_2$ complex	solid-state thermolysis at 400, 500, and 600°C

19	CoS/CNT[118]	$CoCl_2 \cdot 6H_2O$	thioacetamide	solvothermal method at 140°C in N_2 atmosphere
20	Co_3S_4/NCNT[119]	$CoCl_2 \cdot 6H_2O$	Na_2S and thioacetamide	solvothermal method at 160°C
21	$FeCoS_2$/CNT[120]	$Fe(NO_3)_3$ and $Co(Ac)_2$	thioacetamide	solvothermal method at 90°C in an oil bath
22	Ni-Mo-S@C[121]	$Na_2MoO_4 \cdot 2H_2O$ $NiSO_4 \cdot 6H_2O$	L-cysteine	hydrothermal method at 200°C

Interestingly, there are some synthetic methods which are only applicable for supported d-metal/p-block compounds. These methods utilize a support material which already contain the necessary p-block element (either naturally or by additional treatment). For example, Yu et al.[124] report a simple route to prepare in-plane BP/Co_2P, in which CoP nanoparticles selectively grew on the edges of the BP substrate (Fig. 5A), in which Co_2P reacted at the defects of BP nanosheets. Rodríguez-Ramos's group[125] fabricated S-containing CNFs by treating the support in a mixture of H_2S and NH_3 at 1100°C. Following impregnation, a stable Pd-S structure was observed. Supported Pd nanoparticles were also impregnated onto a S-doped polymer [cross-linked poly(N,N'-methylene bis(acrylamide))] and catalytic performance indicated that Pd acted as if there was a strong Pd-S interaction, perhaps indicating sulfidation.[126] A schematic illustration for this system is shown in Fig. 5B. Also, in some selected cases, metal phosphosulfides, such as MnPS,[127] $FePS_3$,[128] and CoPS[129] can also be prepared. The introduction of P and S can be stepwise or simultaneous. For example, S doped CoP/Carbon cloth (prepared by precipitation deposition of $Co(NO_3)_2 \cdot 6H_2O$ with urea) was treated with $NaH_2PO_2 \cdot H_2O$ powder before heating in the presence of S powder at 400°C in N_2 environment to create a mixed p-block element sample.[130] Recently, bimetallic phosphosulfides such as NiFeSP/nickel foam catalysts were further developed.[131]

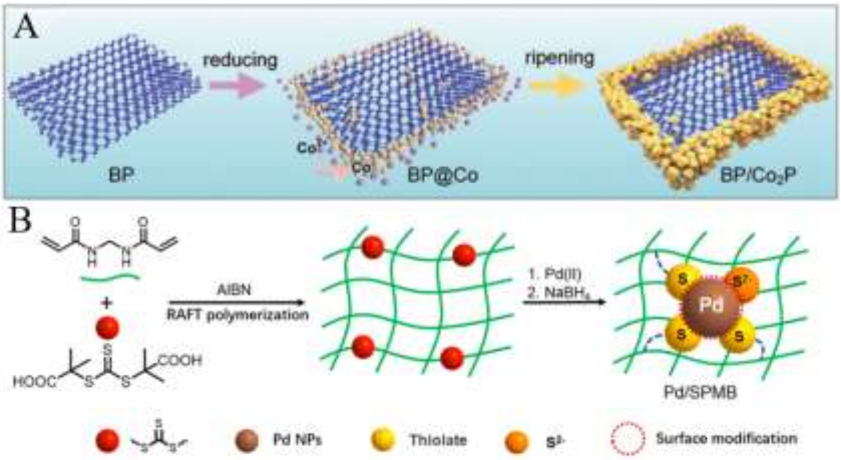

Fig. 5 (A) Schematic diagram of the synthesis mechanism of the BP/Co_2P heterostructures. Reproduced from ref 124. Copyright 2018 Wiley-VCH Verlag GmbH & Co. KGaA, Weinheim. (B) Schematic illustration for the preparation of Pd-S/SPMB. Reproduced from ref 126. Copyright 2019 American Chemical Society.

3. Properties of metal phosphides and sulfides

As described, p-block non-metal elements reacts with a broad range of transition or main group metals to give a diverse class of materials. This is broadly appealing since different metal:non-metal atomic ratios result in unique crystal structures. In other words, different ratios create different geometric arrangements around metal atoms, thus creating an element of site isolation or ensemble design. The nature of bonding changes from ionic for the alkali/alkaline earth elements to metallic/covalent for transition metals and then covalent for the metals in the main group.

3.1 Structural properties

3.1.1 Phosphides

Metal phosphides can form with a broad range of stoichiometries which offers a vast array of structures. For example, at least eight stoichiometries are apparent for nickel phosphide (i.e. metal-poor NiP, NiP_2, NiP_3 and metal-rich Ni_3P, Ni_5P_2, $Ni_{12}P_5$, Ni_5P_4).[132] Measurements from electronic spectra suggest that the oxidation state of P in metal-rich (x > y in M_xP_y, such as M_3P, M_2P) or stoichiometric (x = y in M_xP_y, such as MP) phosphides is P^{-1}, with the ionicity increasing with decreasing metal content.[133,134,135] In contrast, metal-poor (x < y in M_xP_y) phosphides are more appropriately described by covalent bonding where the electrons are localized and this follows the Zintl−Klemm formalism[136,137] and accordingly the P center holds several oxidation states to up to −3.[138] In 1988, Schnering and Hönle et al. provided a comprehensive description of the structures of metal phosphides according to the 'P units' description.[139] Different stoichiometries give rise to disparate arrangements and thus diverse crystal structures (Fig. 6),[48] some of which resemble carbides or nitrides . For example, the structure of MoP is similar to that of WC, where the nonmetal-containing prisms stack together. VP shares the δ-MoN structure with lateral displacement of the prisms by half of the lattice spacing.[140] This is likely to be linked with the phosphorus atomic radii (0.109 nm) which is substantially larger than C or N (0.071 nm; 0.065 nm) meaning that it cannot coordinate well in the common octahedral structure formed by closed-packed metal atoms.[47,48] Instead, trigonal prismatic coordination is more prevalent with small non-metal atoms usually found at the center of this prism surrounded by the metal atoms.[48] In this situation, the introduction of P slightly elongates M−M bonds as compared with the corresponding metal crystal structure.[141] Liu and Rodriguez et al.[142] employed spin-unrestricted DFT calculations to reveal an ensemble effect in Ni_2P, where P effectively dilutes/spaces out surface active Ni sites. Beyond a geometric effect, it is also valuable to consider how the phosphide phase relates to other catalytic systems. In a bimetallic or intermetallic system, the second metal definitely alters surface geometry but both metals still possess metallic character. In the case of a phosphide, the surface P atoms may introduce different character which can lead to the co-existence of both proton-acceptor and hydride-acceptor centers on a single surface. Calculated results also indicate that the M−M distances differs depending on the M/P ratio. Within the PdP_2 structure, neighboring Pd atoms are separated by 280 pm which may imply that these atoms behave as isolated atoms.[99] Whilst many reports have studied bulk properties of a metal phosphide, investigations of surface structure are relatively limited. By employing FTIR studies over bulk and supported Mo phosphides, a CO adsorption band was observed at 2037 cm^{-1} assigned to CO adsorbed linearly on $Mo^{\delta+}$ sites (where $0 < \delta < 2$). This result demonstrated that interaction of CO on Mo terminated surfaces was strong relative to P terminated surfaces, suggesting that catalytic behaviour was associated with the former.[143] Shi and Zhang et al.[144] highlighted that in metal phosphides with higher P content, partial negative charges distributed around P centers on a P-terminated surface, attracts protons as a base which made discharge easier, promoting its application in electrocatalytic reactions. Accordingly, a more detailed understanding of surface structure for these materials would clearly be beneficial for the development of structure performance relationships.

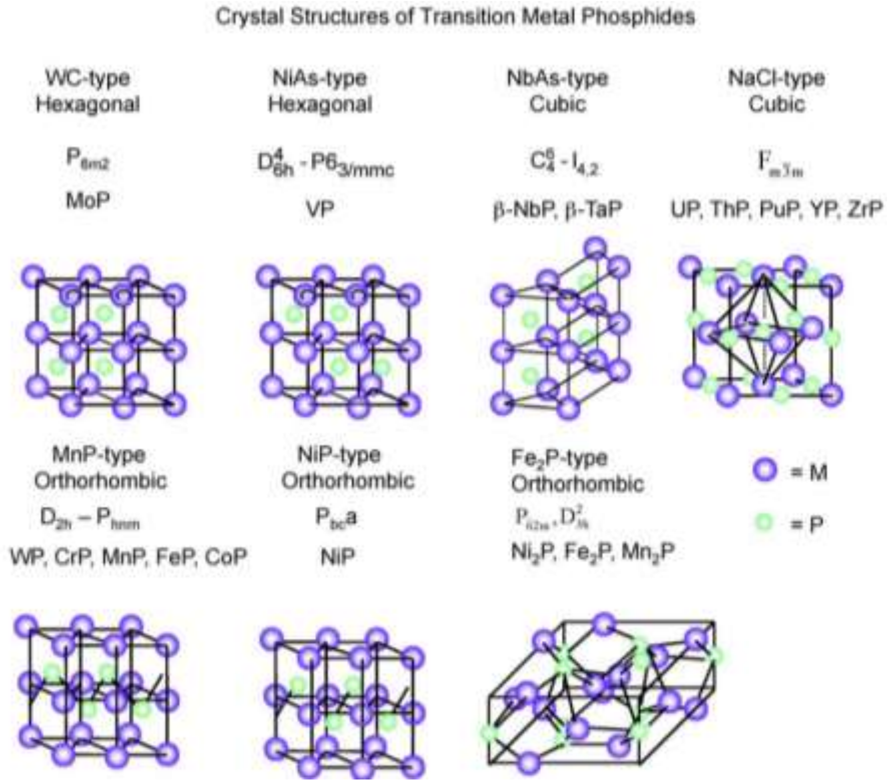

Fig. 6 Structures of some transition metal phosphides. Reproduced from ref 48. Copyright 2009 Elsevier.

3.1.2 Sulfides

Sulfide materials actually show similar physical and chemical properties to the aforementioned phosphides. For example, most metal sulfides and phosphides share metal-metalloid bonds (written as M–S or M–P) with a strong metallic or covalent interaction.[145] The composition and crystal structure of sulfides can also vary widely. For example, the family of Cu_xS_y materials include Cu_2S, $Cu_{1.96}S$, $Cu_{1.8}S$, $Cu_{1.75}S$, $Cu_{1.6}S$, $Cu_{1.39}S$, $Cu_{1.12}S$, CuS and CuS_2 stoichiometries, which in turn determines the active metal distribution on the termination surface.[146] In terms of structure, CuS exists as a hexagonal structure containing layers of CuS_3–Cu_3S–CuS_3 interacting by covalent bonds (Fig. 7A-a).[147] The crystal structure of Cu_2S shows a temperature dependence and exists as a monoclinic structure below ca. 100°C, hexagonal in the range of 100-440°C and a cubic phase is generated beyond 440°C (Fig. 7A b-d).[148,149] The change of crystal structure contributes to different atomic arrangements and a range of electronic properties which would be expected to impact on catalytic properties. Similarly, the Ni–S system also displays a wide range of stoichiometric compositions from Ni-rich to Ni-deficient (i.e., NiS_2, Ni_3S_4, NiS, Ni_3S_2, Ni_6S_5, Ni_7S_6, Ni_9S_8).[150] In separate studies Yu et al. and Idris et al.[151,152] reported that the crystal structures of stoichiometric Ni sulfides also vary with temperature. The hexagonal α-NiS (based on the NiAs structure, a = b = 9.620 Å and c = 3.160 Å, space group P63/mmc) forms at low temperature (140°C) but transforms into the rhombohedral β-NiS structure (a = b = 3.420 Å and c = 5.300 Å, space group R3m,) with only a small increase in temperature (160-180°C). Among the various cobalt sulfides, Co_9S_8, Co_3S_4, and CoS_2 have attracted broad interest. Han et al.[153] presented the crystal structures of a series of CoS_x phases (Fig. 7B). In the pyrite-type CoS_2 structure, Co is octahedrally coordinated with six S atoms but with a mixed oxidation state of Co^{2+}/Co^{3+}. The coexistence of Co^{2+}/Co^{3+} facilitates electron transfer which can thus catalyze transformations (such as decomposition of H_2O_2 to produce a variety of reactive oxygen species). For Co_9S_8, a cubic close-packed structure (a = b = c = 9.927 Å, space group Fm-3m) was reported, in which 8/9 of Co atoms are tetrahedrally coordinated and 1/9 of Co atoms sit at the center of an octahedra.[154,155,156] This phenomenon mean that two distinct metal sites exist in the cubic structure. The rich structural variation observed in sulfides creates a range of interesting materials which maybe exhibit unique catalytic behavior.

The chalcogenides are more widely studied and can form layered structures, thus potentially allowing access to active corner and edge sites which have emerged as the prominent sites for various application. Mo sulfide exhibits a covalently bonded layered structure, with weaker Van der Waals bonding between layers. MoS_2 can crystallize in three crystallographic forms, two of which are naturally occurring (denoted as 2H and 3R) and one is synthetic (denoted as 1T). 2H belongs to the P63/mmc space group,[157] whereas the space groups of 3R and 1T are R3m[158] and P1 space group[159], respectively.

Sn_xS_y, is typical of a main-group sulfide and is composed of double layers of tightly bound Sn–S atoms with Van der Waals interactions between adjacent layers. More specifically, SnS crystallizes with a strongly distorted NaCl-octahedral structure, while SnS_2 forms the layered structure of PbI_2.[160,161]

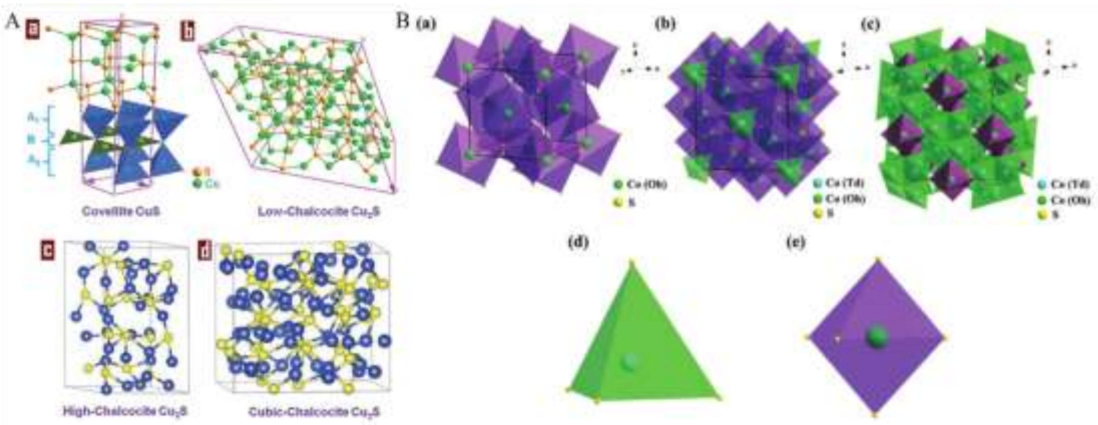

Fig. 7 (A) Crystal structures of (a) covellite CuS (b) low-chalcocite (monoclinic) (c) high-chalcocite (hexagonal) (d) cubic-chalcocite (cubic) Cu_2S. Reproduced with permission from ref 145. Copyright 2014 Royal Society of Chemistry. (B) Crystal structures of (a) CoS_2, (b) Co_3S_4, (c) Co_9S_8, (d) CoS_4 tetrahedron and (e) CoS_6 octahedron, respectively. Reproduced with permission from ref 153. Copyright 2018 Royal Society of Chemistry.

Whilst knowledge of the bulk structure of d-metal/p-block compounds is useful, additional insight into the surface structure is of arguably greater importance for catalysis. It is not uncommon to observe changes in bond lengths and interlayer spacing as a result of surface relaxation effects. DFT calculations offer an effective method for exploring the magnitude of such effects. This is exemplified by the work of Miller et al. who studied Pd_4S surfaces.[162] The crystal structure of Pd_4S was determined experimentally by Gronvold and Rost[163] and a tetragonal unit cell was reported along with expected Pd-Pd (2.78-3.10 Å) and Pd-S (2.34-2.48 Å) bond length ranges. Based on analysis of the bulk structure the S terminated Pd_4S (100) surface would have S atoms which protrude above Pd atoms by 0.46 Å.[140] However, DFT calculations suggest this value decreases to 0.42 Å and is indicative of surface relaxation. Whilst this change may appear small, it is important when considering the adsorption characteristics which underpin catalytic mechanisms. More detailed consideration of the surface chemistry is these materials would be of benefit.

3.2 Electronic properties

The electronic environment of *d block* metals will be influenced by the introduction of light sp heteroatoms via the formation of strong covalent M–X bonds. The difference in electronegativity between the two elements will generally result in a degree of charge transfer from the metal to the non-metal. This influence can be explained according to the Brønsted–Evans–Polanyi relationship, where the interstitial atoms arranged in the right ordering favor alloying.[164,165]

3.2.1 Phosphides and sulfides

Despite many potential applications of metal phosphides in the catalytic field, detailed insight into the electronic structure has remained elusive. Early theoretical studies on Fe, Ni and Co phosphides suggested that back-bonding took place from phosphorus to metal atoms which would contribute to a positively charged P,[166] although appears contrary to the difference in electronegativity. On account of the catalytic behavior being strongly dependent on the degree of P back-bonding and the occupancy in 3d states of the metal, an unambiguous understanding of the electronic properties of phosphide systems is required. The electronic properties are expected to be influenced by the electronegativity difference, the ratio of M to P as well as the localised environment. Mar et al.[135] examined the electronic structures of binary MP, M_2P and M_3P phosphides (where M = Cr or Ni) by means of experiments including X-ray photoelectron and absorption spectroscopy. The binding energy of phosphorus 2p3/2 and the energy of absorption decreased linearly with increasing difference in electronegativity which implies improved charge transfer from the metal to P atoms (estimated formal charge of -1). As mentioned already, the electronic structure of Ni_2P was evaluated by XPS and XANES. Measurements suggest that the BE is much smaller in Ni phosphides than those of oxidized species (Ni_xO and P_2O_5) which suggests Ni−P bonds tolerate lower ionicity than Ni−O bonds (associated with lower difference of electronegativity).[48,141] Furthermore, the P centers in metal-rich phosphides adopt the oxidation state of -1, although the ionic character tends to increase with increasing P content meaning that P-rich phosphides have valence electrons that are more localized. Consequently, P can hold several oxidation states from 0 to −3.[139] Interestingly, the electronegativity of P is relatively low (2.19) compared with that of other light sp elements such as sulfur (2.58), carbon (2.55) and nitrogen (3.04) and therefore the electrons are to a certain extent localized in the vicinity of P atoms,[23] leading to semiconductor or insulator properties. By analyzing the electronic structures, for instance, of a series of Co–P compounds, Yang et al.[133] analyzed the charge density distribution of Co_xP_y. Fig. 8 a–d displays the total charge density map in the (010) plane for Co_2P(I), (100) plane for Co_2P(II), (010) plane for CoP, and (011) plane for CoP_2, respectively. It is clearly seen that weak covalent bonding exists between Co and P atoms, originating from the interactions of s–p hybridization. Meanwhile, it can also be observed that the charge density around P atoms shows a strong directional distribution toward Co atoms with significant charge distribution overlap between Co and P atoms in all samples, illustrating the existence of covalent bond between Co and P atom. Based on the density of states (DOS) result, the lowest valence band of Co_2P and CoP mostly constitutes P 3s character, while the upper valence band is comprised of hybridization of Co 3d and P 3p. No band gap near the Fermi level can be observed, suggesting metallic nature of Co_2P and CoP for metal rich materials whereas the P-rich CoP_2 and CoP_3 compounds possess semiconductor character based on the DOS at the Fermi level. Furthermore, it is clear that the p–d hybridization of Co 3d and P 3p character gets stronger with increasing of P content.

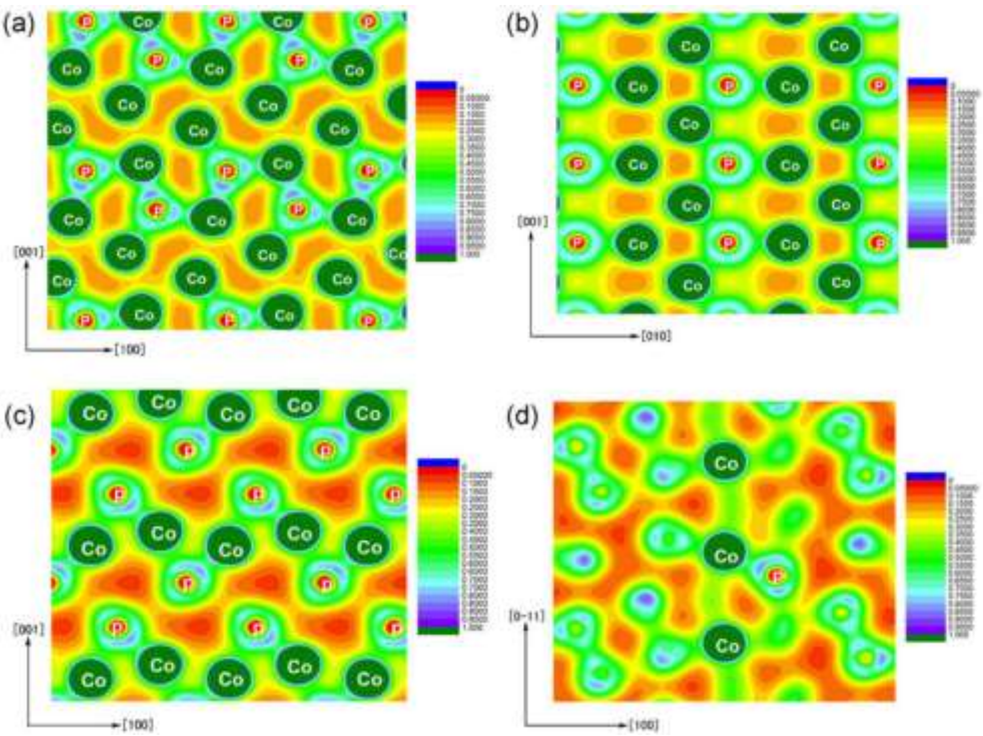

Fig. 8 Distribution maps of total charge densities in the (010) plane of Co_2P (I) (a) and CoP (c), (100) plane of CoP (II) (b), (011) plane of CoP_2 (d). Reproduced with permission from ref 133. Copyright 2010 Elsevier B.V.

Over past decades, the metal sulfides have attracted wide attention owing to their interesting electronic properties. The electron-rich S is expected to alter the electronic state of a transition metal containing compound. For example, p−d orbital hybridization between S and Re atom,[167,168] leads to charge compensation from S p-obritals to σ Re−Re bonds which thus changes the optimized electronic states. This was confirmed by Li and coworkers via calculation of the projected d-band densities of states. Moreover, metal defect introduction, activates S and Re−Re bonds through the formation of dangling bonds (Fig. 9) which achieve better catalytic activity.[169] The same phenomenon was reported in the MoS system. The effect of sulfur modification on the electronic properties extends to noble metals. Albani et al.[170] formed supported Pd_3S nanoparticles by inducing S into the Pd lattice after a mild treatment. According to theoretical calculations, incorporation of S resulted in a downshift of the d-band DOS for Pd_3S (202) and Pd_3S (001) to –1.80 and –1.90 eV (relative to the reference value for Pd of −1.39 eV). This was in agreement with XPS observations and illustrates a shift in charge away from Pd. Song et al.[171] reported that NiS_2 possessed typical semiconductor properties where the intrinsic charge compensation from S to Ni could manipulate the active electronic states. In a study by Subbaraman et al.[172], it is stated that Ni^{2+} is more active than other divalent cations (Co^{2+}, Fe^{3+}, Mn^{2+}) and this is ascribed to the enhanced 3d−2p repulsion between the d-band of metal and p-band of the coordinated electronegative ligand (S^{2-}). Another example is Al_2O_3 supported M-Mo-S (M=Co or Ni),[173] in which the second metal atoms are generally located at the edges of MoS_2. It is found that Co or Ni play a role of electron donor to Mo atoms, weakening the bond of Mo-S, and consequently producing S vacancy sites which play a key role in hydrodesulfurization processes.

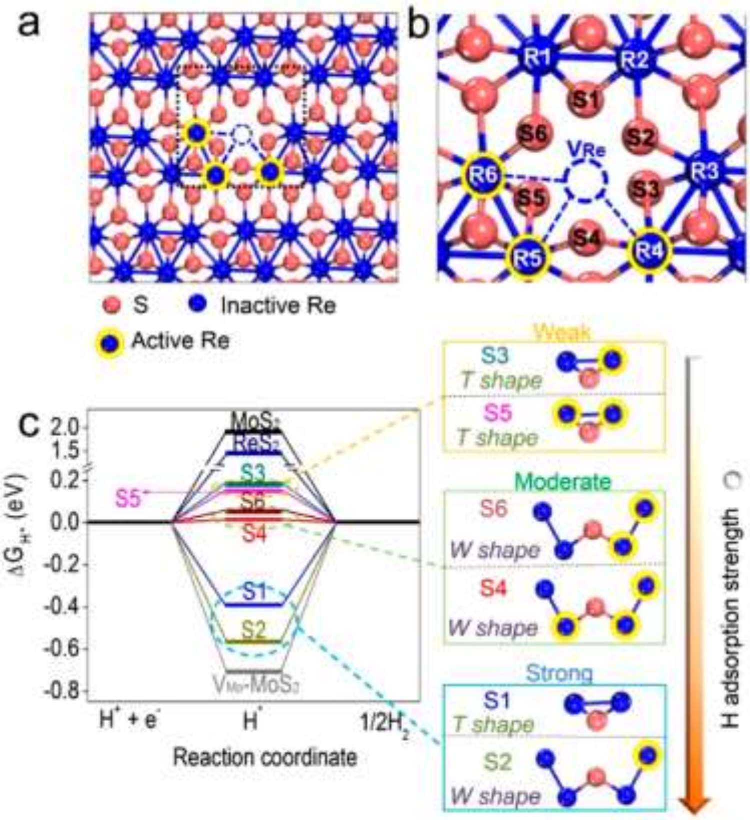

Fig.9 (a) The optimized structure and (b) enlarged defect structure. (c) ΔG (H*) in six exposed S atoms around V_{Re} in V_{Re}−ReS_2, ReS_2 without Re vacancy. Reproduced with permission from ref 169. Copyright 2018 American Chemical Society.

In addition to the phosphide and sulfide phase, the nature of the support generally plays a key role in the morphology, dispersion, and obviously in the catalytic activity of the prepared catalysts. For example, Lercher et al.[174] reported an unsupported Mo sulfide catalyst formed slabs with 15-20 nm particle size, whereas supporting on a γ-

Al_2O_3 phase generated a highly stable dispersed Mo sulfide with average stacking degree of 1.6-1.9 nm. The support therefore facilitated higher dispersion which in turn increased the proportion of active metal surface atoms and improved catalytic performance. Besides, well-known that conventional supports are not a totally inert substrates under reaction conditions (such as acidic character) and could allow the migration of the active metals into its more external surface forming sub-superficial spinels.[175] In early reports, Topsøe et al.[176] found that the CoMoS structures possessed more intrinsic activity once considerably decreasing the interaction with Al_2O_3 substrate. Since then, the modulation of the interaction between the active phases with support has been triggered the wide attention. Moreover, it is further realized that the catalytic behaviour of MoS_2 materials is strongly dependent on the morphology and the orientation, associating with the bound on the edge or basal planes decided by the interaction with the support.[177] For instance, the preferential bonding is on the (111) and (100) planes when carrier is selected as γ-Al_2O_3, as the relatively weak and intermediate interactions as Bara et al. reported,[178] while the plane (110) presented highly dispersed and oriented oxide particles with strong metal support interaction with small stacked MoS_2 slabs.

3.3 Properties of other d-metal/p-block materials

Transition metals can also react with other p-block elements such as boron, carbon or nitrogen to obtain the corresponding borides, carbides and nitrides. These materials also display a large range of diversity in terms of composition and structure. Whilst detailed discussion of carbides and nitrides fall out with the scope of this review,[179] it's worth noting that when the radii ratio of non-metal to metal (r_x/r_M) is greater than 0.41 and less than 0.59, geometric structures are considered to be more stable (Hagg's rule).[180] In the case of borides, as the metal to boron ratio decreases, the evolvement of boron structures from 1 and 2D clusters to extended 3D frameworks occurs. Nickel borides are a fair example of a class of metal borides (MB's)[181], in which a boride layer mainly consists of Ni_2B and NiB, in which the former incorporates short linear B−B chains, while the latter is composed of corrugated B−B bonds, in agreement with that of monoclinic Ni_4B_3. The difference in Ni_3B is the presence of longer B−B interatomic distances, which suggest the boron atoms in this Ni trigonal prism are isolated. Tungsten borides show similar diversity. In the case of W_2B, the W_2B–W_2B structure becomes the most stable, in which a W atom is fourfold coordinated by B atoms and surrounded by three W atoms, while B atoms are coordinated with eight W atoms located at the corners of an archimedian square antiprism.[182] Totally different from W_2B, WB-WB structures in WB are made of trigonal prisms consisting of W atoms along with the B atoms located at the body center. This WB_2 structure is also based on a monocapped trigonal prism arranged with eight B atoms surrounding the W atom, with the sevenfold coordinated B atom surrounded by four W atoms and three B atoms. Recently, Wang and coworkers presented work on ternary transition metal borides (such as Ti_2InB_2 and Ti_2SnB_2) based on both theoretical and experimental studies.[183] These borides crystallize with a hexagonal structure as opposed to the orthorhombic one. For the LaB_6, 6xB atoms form an octahedra occupying the corners of a simple cubic lattice.[184]

In the case of metal borides, the diverse electrical properties mirror the complex chemical bonding behavior. Our understanding of charge transfer between the boron and transition metal is still highly questioned in view of first principle calculations and photoelectron spectroscopy.[185] Specifically, first principle calculations[186,187] suggest total electron shift from the metal to boron based on the relative electronegativity. However, the d electrons are, more often than not, incompletely polarized in the opposite direction, leading to increased d electron population of the metal atoms. Until recently, researchers proposed differing electron transfer including from boron to metal for boron-poor TM borides (MB_x, $x \leq 2$) and from metal to boron for boron-rich TM borides (MB_x, $x \geq 2$). The electronic structure of a NiB material was examined experimentally and by calculations. The results confirmed transfer from B to Ni[188,189] originating from hybridization of s−d orbitals in the metal and s−p orbitals of boron. Ma et al.[190] explored boron-rich Mo systems including MoB_2, Mo_2B_5, MoB_3 and MoB_4. Based on total and partial density of states, the major orbital occupancy near the Fermi level stems from Mo 4d electrons, suggesting metallicity, while significant hybridization between the Mo 4d and B 2p orbitals results in a strong Mo-B covalent bonding nature. Additionally, back-donation indeed occurred for all the compounds. It is noteworthy that the same conclusion was obtained for both ZrB_2 and HfB_2 where the bonding states of Zr/Hf-d and B-2p orbitals are responsible for the existence of covalent bonding.[191]

Interstitial carbides and nitrides are frequently investigated together because of the similarity in structure, although these structurally differ from both phosphides and sulfides. This is related to the atomic size of C (0.071 nm) or N (0.065 nm) which enables occupation of interstitial sites between metal atoms.[192] There is presently interest in binary molybdenum or tungsten-based materials.[140] The molybdenum carbides display simple crystallographic structures.[193] The β-Mo_2C is reported as a hexagonal closed packed structure, whereas α-MoC_{1-x} is face centered cubic. Demczyk and coworkers found that the surface structure of passivated Mo_2N differed from the underlying structure from the bulk material, while δ-MoN adopted the NiAs structure but with a series of closely related structural variants.[194]

3.4 Implications of properties for catalysis

The above observations/remarks suggest the inclusion of additional non-metal C, N, P or S atoms can be beneficial for controlling and tuning metal reactivity. By bonding heteroatoms to transition metals, changes in electronic properties are induced and/or the geometry around the metal changes which could create unique behavior for catalysis. In the terms of modulating geometric structure, the introduction of p-block elements dilutes the transition metal atoms in a controlled manner if a single phase is formed (i. e., Ni_2P or Ni_5P_4).[38] For example, detailed analysis reveals the presence of spatially isolated nickel trimers which modifies the binding energies of organic intermediates and assists in preventing undesired side reactions.[38] This type of uniform surface site is difficult to achieve in a bimetallic catalyst since a number of factors can influence the distribution of the two components. Whilst in principle, an intermetallic system may yield uniform surface sites, the second metal may not be inert (i.e., the surface may still seem like a contiguous surface). By changing the M:P block ratio it is possible to explore a variety of surface architectures. For example, the group of Wei changed the geometry around active Ni sites by adding P, to explore the impact on the adsorption state and hydrogenation of a C-C triple bond.[195] DFT calculations suggested that the long distance of Ni−Ni in Ni_2P inhibited the orbital hybridization of C=C from sp^2 to sp^3, and thus di-π(C=C) adsorption occurs on a single nickel atom, rather than dissociated di-σ(C=C) adsorption on multiple Ni atoms.

Electronic behavior also has an important effect on reactant adsorption. Through experimental and theoretical methods. Liu et al.[171] showed that intrinsic charge compensation from non-metal heteratoms to metal bonds could influence active site electronic properties, such that reactants like hydrogen adsorb with different strengths which could improve catalytic traits. Furthermore, reports illustrate that catalytic activity can be enhanced as a function of the content of heteroatoms (i.e. B) which is attributable to the electronic influence of that heteroatom on the active metal.[196,197] For example, a range of Ni:B ratios were reported by Acosta et al.[198] for the hydrogenation of nitrobenzene and glucose. They found that the non-metal atoms introduced holes into the Ni metal d band, which modified the electron population of the Fermi level, altering the rate for dissociative chemisorption of hydrogen. More importantly, the interaction between the transition metal and metalloid element led to an electron-deficient metal and also generated a high energy barrier for subsurface species (i.e. hydride formation).

4 Catalytic applications of metal phosphides and sulfides

Metal phosphides and sulfides have been explored as potential catalytic materials for various reactions, particularly for processes which are typically catalyzed by metals. In some cases, the metal phosphides/sulfides may possess acid-base properties, redox reversibility, capacitance, optical properties or high electric conduction, broadening their potential range of applications. In this section, the focus is on the application of these materials in processes including alkyne hydrogenation, hydrodesulfurization (HDS), hydrodenitrogenation (HDN) and electro-/photo-catalysts for energy conversion.

4.1 Gas phase alkyne hydrogenation

For many decades metal phosphides have been explored for gas phase alkyne hydrogenation with the first studies reported in 1974 by the group of Sauer, who investigated the hydrogenation of acetylene to ethylene reaction using Ni and Rh phosphides.[26] Ni_2P was also reported to possess good catalytic performance for the hydrogenation of butadiene to butane by Nozaki and co-workers in the 70s and 80s.[199,200] However, the application of analogous materials featuring a precious group metals such as Pd remained less well studied. Inspired by this, our group[99] developed a series of TiO_2 supported Pd phosphides (including Pd_3P and PdP_2 phases) with a small particle size of 4.0 nm using $NH_4H_2PO_2$ as phosphorous source. The catalytic results showed that PdP_2 exhibits enhanced catalytic behavior in comparison with Pd_3P for the hydrogenation of acetylene under both non-competitive and competitive conditions (i.e., with or without ethylene co-fed along with acetylene). CO-FTIR characterization indicated the incorporation of P helped to break up contiguous Pd sites (creating a more discrete type of Pd site), with this effect being more pronounced for PdP_2 than Pd_3P (Fig. 10). This geometric alteration then in turn, effects the adsorption and desorption of reactants/products and thus leads to improved activity and selectivity, relative to monometallic Pd/TiO_2 catalysts.[201] In addition, no evidence of deactivation for the PdP_2 phase was observed for a longer 50 h time on stream test. Gas phase alkyne hydrogenation catalysts tend to deactivate through alkyne oligomerization which leads to blockage of active sites. Given that oligomerization occurs *via* alkyne coupling which would require more than one adjacent adsorption site, it is perhaps not surprising that Pd sites which are essentially diluted/spaced out by P atoms offer good stability.

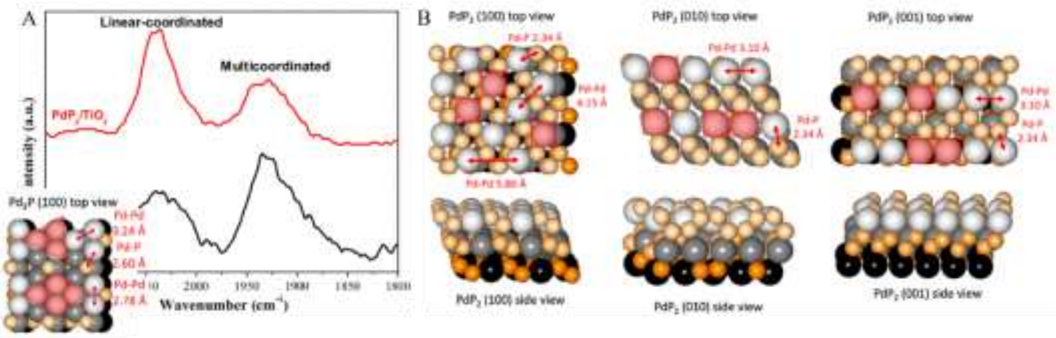

Fig. 10 (A) In situ FTIR spectra of palladium phosphide catalysts exposed to CO. 2% Pd_3P/TiO_2 (lower, black) and 2% PdP_2/TiO_2 (upper, red). (B) Structures of PdP_2 (1 0 0), (0 1 0) and (0 0 1) surfaces based on the crystal structure. Reproduced from ref 99. Copyright 2018 Elsevier.

Metal sulfides have also been explored by our group for gas phase alkyne hydrogenation with a particular focus on palladium sulfide based materials. A series of unsupported, bulk phase samples were prepared by exposing an amorphous commercial PdS sample to hydrogen.[67] During reduction at temperatures ranging from 150°C to 350°C, the sample lost sulfur, crystallized and underwent a gradual phase change to a sulfur lean Pd_4S phase (via an intermediate $Pd_{16}S_7$ phase). The Pd_4S phase displayed excellent catalytic performance for acetylene hydrogenation with exceptionally high ethylene selectivity. The strong catalytic properties were attributed to a site isolation effect originating from the crystal structure of Pd_4S. Although, it is also thought that the change in Pd electronic state as a result of the metal-chalcogenide bonding favored ethylene desorption. This therefore highlights how d-metal/p-block compounds can lead to both interesting geometric and electronic properties. Although a bulk phase PdS powder does not represented an efficient utilization of the expensive Pd metal, it serves as a method for establishing clear structure-performance relationships and highlights the value of the literature described in section 2.1 of this review.

Based on the need to more effectively utilize Pd, an equivalent material was prepared on a carbon nanofiber support (note: detailed characterization by a variety of techniques confirmed the same Pd_4S phase was present).[122,202,203] With the supported sample, ethyne or propyne (in the presence of the corresponding alkene) could be converted with 95% and 86% alkene selectivity at full alkyne conversion which exceeds what was achievable with a zero-valent Pd catalyst.[202] Like with the equivalent bulk phase sample, this was related to the crystal structure of Pd_4S which is thought to result in Pd atoms which predominantly possess S atoms as the nearest neighbors to realize the effective isolation relative to the ensembles in monometallic Pd catalyst (Fig. 11A).[202] The state of the art catalytic performance also extended to the elevated pressures required for industrial application (80% ethylene or 85% propylene selectivity, see Fig. 11B) and the formulation could be prepared with an egg-shell type distribution in pelletized form.[203] As with the Pd phosphide catalysts, no signs of deactivation were observed over Pd_4S sample for either bulk or supported samples. Other bulk phase sulfides (i.e. Ni_2S_3 and CuS) were explored and whilst the nickel analogue was observed to be active it was less selective for acetylene hydrogenation.[203] Furthermore, the supported Pd_4S phase was also studied in the partial hydrogenation of but-1-yne and but-2-yne to probe the difference between external and internal alkynes. Regardless of the nature of the alkyne, Pd_4S offered exceptional alkene selectivity (92–93%). DFT calculations were used to gain insight into the reaction mechanism (Fig. 11C) and indicted that the reaction involved two Pd atoms which are separated from other Pd atoms by neighboring S atoms. It is perhaps important to highlight here that the role of the P-block element in this example is to create isolated sites, not necessarily isolated atoms. The calculations also suggested the energy barrier for alkene desorption over Pd_4S is lower than that for alkene hydrogenation.[204]

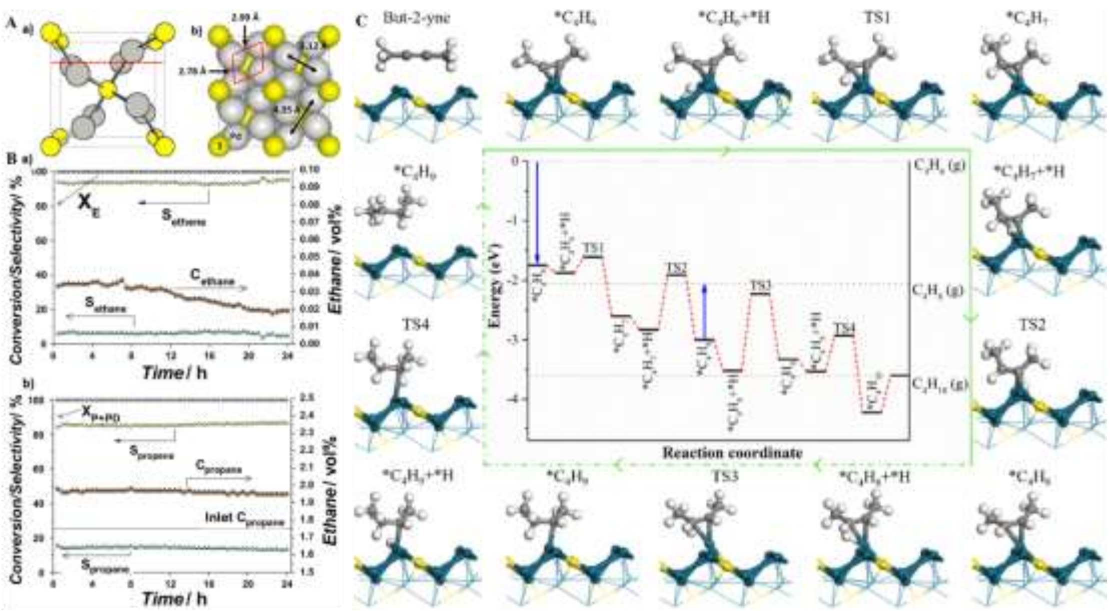

Fig. 11 (A) Pd_4S unit cell viewed along the (001) plane. Reproduced with permission from ref 202.

Copyright 2017 Elsevier Inc. (B) Conversion, product selectivity versus time over Pd_4S/CNF in (a) ethyne/ethane mix and (b) propyne/propadiene/propene/propane mix. Reproduced with permission from ref 203. Copyright 2016 Elsevier Inc. (C) Step-by-step hydrogenation mechanism of but-1-yne to butane on the Pd_4S (200) surface. Reproduced with permission from ref 204. Copyright 2020 Elsevier Inc.

4.2 Liquid phase hydrogenation of functionalized alkynes

On the other hand, metal–metalloid materials are also promising candidates for the liquid-phase hydrogenation of functionalized alkynes. Nickel phosphides were once fabricated by Corma and coworkers as a cheap and mild catalyst for the chemoselective hydrogenation of alkynes such as undec-5-en-1-yne and p-(1-phenyl-ethynyl) styrene. to cis-alkenes but with lower reactivity and Z/E ratio for internal alkenes.[205] The Ni:P ratio was reported to be important with ratios of 3.5 or greater meaning that P blocked the most unsaturated sites (acting as a poison) and also resulted in electron transfer from Ni to P. Supported Ni–P nanoparticles including $Ni_{12}P_5$, Ni_2P, and NiP_2 derived from hydrotalcite precursors have been also explored for the chemoselective hydrogenation of phenylacetylene.[195] The resulting Ni_2P/Al_2O_3 sample exhibited much better styrene selectivity (up to 88.2%) than $Ni_{12}P_5/Al_2O_3$ (48.0%), NiP_2/Al_2O_3 (65.9%) and Ni/Al_2O_3 (< 1%) catalysts. *In situ* CO-IR, EXAFS and DFT calculations revealed that the incorporation of P extended the Ni-Ni bond length to 0.264 nm (Ni-Ni = 0.249 nm for pure Ni) and withdrew electron density from Ni to create an electron deficient Ni site ($Ni^{\delta+}$). The combined geometric and electronic effects favored alkene desorption although employing ethylene as a model substrate (Fig. 12).

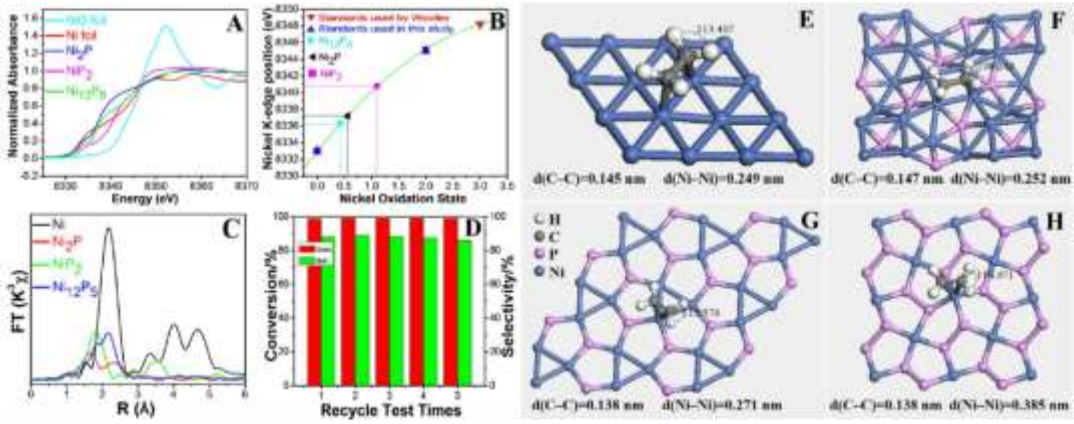

Fig. 12 (A) Normalized intensity of Ni K-edge XANES spectra (B) Ni K-edge position plotted against Ni oxidation state (C) Fourier transform k^3-weighted EXAFS spectra in R space (D) The catalytic conversion and selectivity vs cycle number for the hydrogenation of phenylacetylene over Ni_2P/Al_2O_3 catalyst at 100°C; Atomic arrangement and chemical bonding of the preferential crystal face of (E) Ni (111) face, (F) $Ni_{12}P_5$ (001) face, (G) Ni_2P (001) face and (H) NiP_2 (001) face showing the optimum adsorption state of ethylene (used as a model in place of styrene). Reproduced with permission from ref 195. Copyright 2015 American Chemical Society.

Subsequently, Ni_2P and Ni_5P_4 active phases were further assessed in the hydrogenation of 1-hexyne and 2-methyl-3-butyn-2-ol.[38] It was found that the activity and selectivity in the semi-hydrogenation of 1-hexyne over Ni_2P and Ni_5P_4 didn't link to the Ni/P ratio. However, in the case of 2-methyl-3-butyn-2-ol the Ni_2P based sample exhibited a higher rate and lower selectivity. The P atoms were shown to create spatially isolated Ni trimers which were beneficial for the desorption of alkene relative to a Ni only catalyst (Fig. 13A and B). Zhao et al.[206] fabricated ultrasmall Pd–P NPs by reduction of $Pd(acac)_2$ and TPP as P source and tested the catalysts for performance in the chemoselective hydrogenation of various terminal and internal alkynes. Electronic deficient Pd was observed by XPS as a positive shift of BE of Pd (3d) relative to that in monometallic Pd nanoparticles. This hindered the formation of palladium hydride and this was linked to the excellent semi- and stereo-selectivity to alkene product. Pd-P nanoparticles can be also obtained by low-temperature reduction of $Pd(acac)_2$ in the presence of P and H_2, as reported by Belykh et al. for the hydrogenation of mono- and di-substituted acetylenic compounds.[207] By varying the P:Pd ratio, the triple bond hydrogenation rate, relative to the double bond hydrogenation rate increased, resulting in a significant boost in activity (8–9 fold), while maintaining high selectivity to the corresponding alkenes. The same group also studied 2-methyl-3-butyn-2-ol hydrogenation as a model substrate[208] and found modification with P improved the activity and turnover number (relative to Pd catalyst) without any decrease in the selectivity to 2-methyl-3-butene-2-ol at high conversion (95-98%). Furthermore, the group of Zhao[209] investigated bimetallic (and trimetallic) phosphides of Pd−Cu−(Ni)−P and explored the relationship between composition, morphology and catalytic behavior for diphenylacetylene, and 1-phenyl-1-butyne hydrogenation. The excellent catalytic activity and selectivity was attributed to synergistic effects between Pd and P as well as the another metals (Cu or Ni) which lead to electron deficient of Pd. The excellent performance of Pd sulfides for gas phase hydrogenation, described earlier, also extends to liquid phase alkyne hydrogenation. Specifically, Albani et al. demonstrated excellent activity, selectivity and stability for a Pd_3S/C_3N_4 catalyst for the liquid phase hydrogenation of 2-methyl-3-butyn-2-ol. [210] A molecular level understanding for Pd_3S/C_3N_4 was obtained through a combined experimental and DFT approach which revealed the stellar catalytic behavior was linked to spatially-isolated Pd sites relative to Pd metal (Fig. 13C). Importantly, this type of active site exists as a result of the underlying Pd_3S structure. Beyond this particularly ensemble, the S atoms were shown to impart a bifunctional mechanism by weakening binding of the organic intermediates. The report also compared the Pd_3S and Pd_4S phases and suggested that whilst they were similar, the Pd_3S phase, was more active for 2-methyl-3-butyn-2-ol hydrogenation. This type of comparison is important because if the underlying surface structure of the d-metal/p-block compound controls the active site geometry, then it is perhaps not surprising that changes in substrate structure would reveal a preference for different active sites. In other words, changing the d-metal/p-block element stoichiometry offers a feasible and reproducible method by which the active site geometry can potentially be fine-tuned.

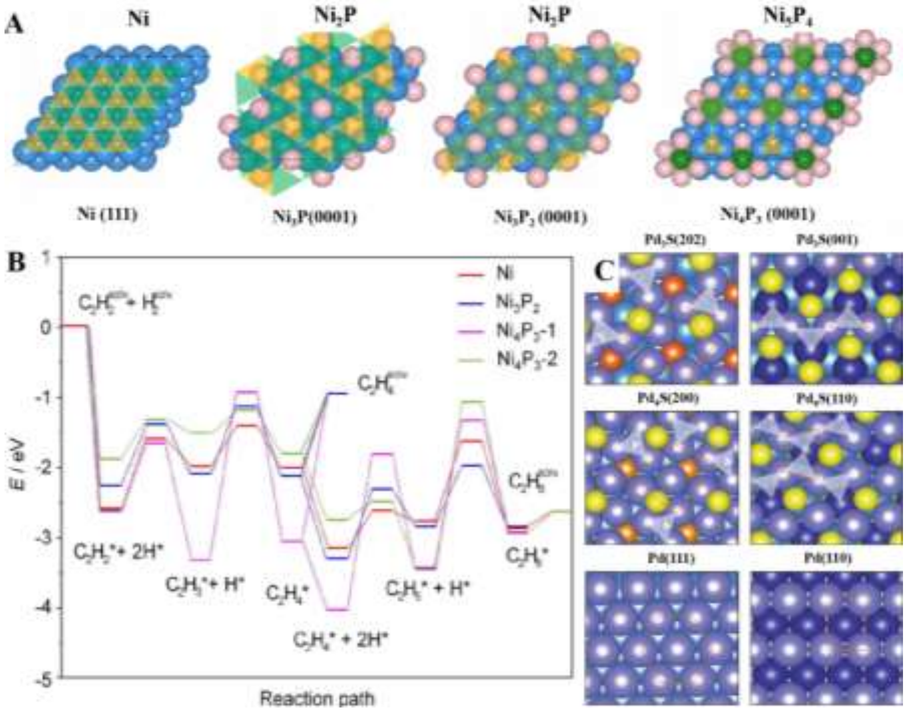

Fig. 13 (A) Top view of the Ni (111), Ni_2P (Ni_3P (0001)), Ni_3P_2 (0001) and Ni_5P_4 (Ni_4P_3 (0001)) surface termination. (B) Energy profiles for the hydrogenation of acetylene on the Ni(111), Ni_3P(0001), Ni_3P_2(0001) and Ni_4P_3(0001) surfaces. Ni_4P_3-1 and Ni_4P_3-2 indicate that the profiles consider two different adsorption configurations of the acetylene molecule, forming P-CH-CH-P and P-CH-CH-Ni intermediates, respectively. Reproduced from ref 38. Copyright 2018 Wiley-VCH Verlag GmbH & Co. KGaA, Weinheim. (C) Structure of Pd_3S and Pd_4S highlighting 'Pd ensembles' (as triangles in the image) and a comparison to pristine Pd surfaces. Reproduced from ref 210. Copyright 2018 Nature.

4.3 Other reactions

Supported phosphides were originally developed for catalytic applications such as hydrodesulfurization (HDS) or hydrodenitrogenation (HDN).[144] For instance, in 2005, Liu et al.[211] investigated a Ni_2P catalyst for HDS using thiophene as a representative reactant. P atoms in Ni_2P were shown to play a complex and important role. First and foremost, a ligand type effect arose from the formation of Ni–P bonds which contributed to a high ability to dissociate both thiophene and hydrogen. Secondly, an ensemble effect (created by the introduction of P relative to monometallic Ni catalyst) decreased the number of active sites but then suppressed deactivation caused by high coverage of the strongly bound S. The P atoms also offered effective bonding for the thiophene and H atoms necessary for hydrogenation. A similar mechanism/interpretation has also been suggested for HDS[43] over MoP and for hydrodehalogenation reactions over Ni_2P materials.[212,213] Furthermore, by monitoring the CO-FTIR spectrum, a blue shift from 2045 cm^{-1} to 2100 cm^{-1} occurred over a MoP/SiO_2 catalyst during the process of hydrodesulfurisation, indicative of partial sulfidation of the surface suggesting the potential formation of a multi p-block compound.[214]

Regardless of whether used in HDN or HDS reactions, one crucial feature of Ni phosphide catalysts is bifunctionality - metallic sites on Ni phosphide and acid sites generated by residual phosphate on the support surface.[46,215] This bifunctionality can be regulated by the changing the initial ratio of P to Ni. To take advantage of this, Zhang and coworkers[216] explored supported nickel phosphides with different initial Ni/P molar ratios (Ni/P = 1:3, 1:2, 1:1, and 1:0.75) as efficient one-pot conversion catalysts for the cellulose to sorbitol reaction. The dual-site function was responsible for the hydrolysis of cellulose to glucose and the subsequent hydrogenation of glucose to sorbitol in a very high yield. Similarly, Fukuoka et al.[217] also employed the same nickel phosphide catalysts for the conversion of cellulose in water. Over 60% sorbitol production was obtained with high cellulose conversions. However, in contrast to Zhang's conclusion, an amorphous Ni phosphide phase was identified with increasing temperature, which was considered to be responsible for the high yield. Guaiacol can be employed as reactant since it is an excellent model compound for species derived from the lignin fraction of biomass. The hydrodeoxygenation (HDO) of guaiacol was also investigated over Ni_2P supported on various acidic supports.[218] The order of activity of Ni_2P catalysts was amorphous silica–alumina > USY zeolite embedded in a silica–alumina matrix > the microporous zeolite ZSM-5. The phosphide catalysts produced cresol and phenol products as the main products whereas, in contrast, a SiO_2 supported catalyst favored benzene formation. This implies that the acid sites influence the product distribution. Contact time measurements revealed that the main pathway for the most active Ni_2P/amorphous silica-alumina sample involved conversion of guaiacol to the primary intermediate catechol before dehydroxylation to phenol. Furfural is another biomass-derived platform molecule of interest. The gas-phase HDO of furfural to yield value added products such as 2-methylfuran (MF) was explored over transition metal phosphides. Ni_2P was found to be the most promising catalyst although varying the Ni:P ratio was reported to influence selectivity to MF and tetrahydro-2-methylfuran.[219] Increasing P content appeared to weaken the interaction between the furan ring and catalyst compared with the conventional zero-valent Ni metal, which then contributed to less ring opening and ring hydrogenation activity. Interestingly, a smaller Ni:P ratio also improved the interaction of the carbonyl group which enhanced its conversion (note: electron-deficient $Ni^{\delta+}$ binds to the lone pairs of carbonyl O and the electron-rich $P^{\delta-}$ donates electrons to the antibonding orbitals of C=O derived from XPS and IR analysis-Fig. 14A and B). Importantly, P species can also act as Brønsted acid sites which facilitate C_1-O_1 hydrogenolysis of furfuryl alcohol to increase MF yield, but a similar phenomenon is not observed in monometallic Ni catalyst (see Fig. 14C). Golubeva et al.[220] investigated in situ generation of nickel phosphide particles. Ni_2P and $Ni_{12}P_5$ phases were synthesized using oil-soluble precursors in toluene and water-soluble precursors in ethanol, respectively. Both catalytic systems exhibited high activity in the hydroprocessing of furfural. Notably, using toluene as a solvent, 2-methylfuran was obtained as main product (highest selectivity of 77%), whereas ethyl levulinate and 2-methylfuran were obtained with selectivity of 40% and 38% respectively when ethanol was used a solvent. This can be ascribed to the existence of both metal and acid sites for the catalyst formed in the ethanol system (note: the hydrogen donor properties of ethanol are also expected to play a role).

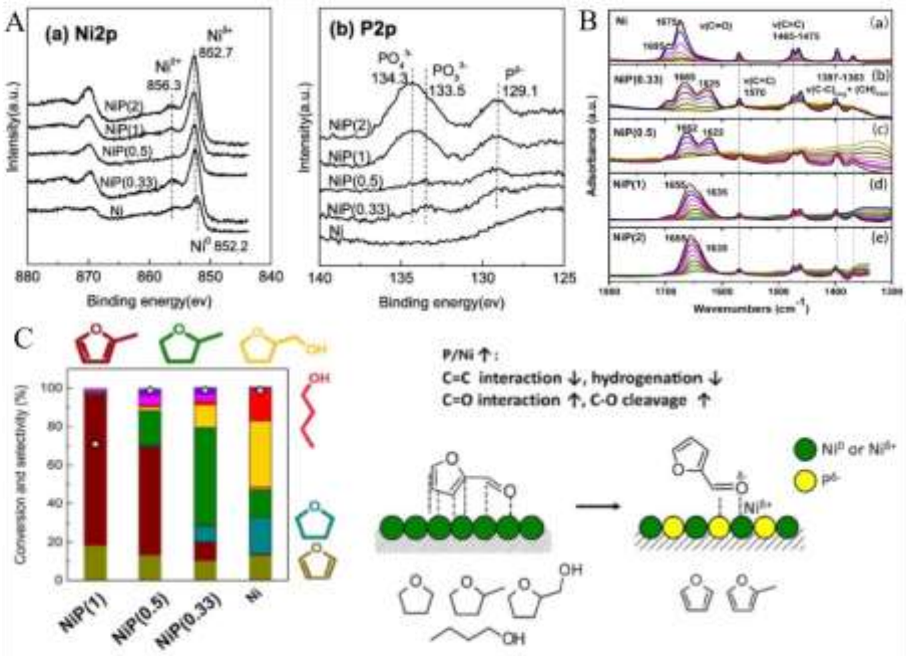

Fig. 14 (A) (a) Ni 2p and (b) P 2p core-level XP spectra of reduced NiP(x)/SiO_2 (x =0, 0.33, 0.5, 1, and 2) (B) IR spectra of furfural adsorbed on reduced NiP catalysts (C) Effect of P on furfural HDO over Ni and nickel phosphide catalysts (Catalyst=60 mg, T =180 ℃, H_2=20 ml/min, furfural=0.001 ml/min in liquid). Reproduced with permission from ref 219. Copyright 2021 Elsevier Inc.

Hu and coworkers[221] studied the hydrogenation activity of a bulk Ni_2P sample using 1.5 wt.% heptene in toluene and 1.0 wt.% phenylacetylene in ethanol. This catalyst displayed low activity but could be tuned by introducing TiO_2 or CeO_2 additives in a controlled amount. Gao et al.[222] reduced the particle size of Ni_2P to sub-nanosized clusters with P-doped carbon for the chemoselective hydrogenation of nitroarenes. It was found that electron transfer from P-doped carbon to the Ni_2P clusters caused a downshift of the d-band center of Ni which promoted H desorption on highly charged antibonding orbitals of Ni−H. Meanwhile, the nitro group was preferentially adsorbed on the surface of P-doped carbon owing to geometrical hindrance on Ni_2P clusters that contributed to good selectivity. Very recently, a single Ni_2P phase was employed as a novel non-noble-metal catalyst for the hydrogenation of nitrate to NH_3 under ambient conditions.[223] The introduction of P contributes to the Ni_2P (001) facet possessing an H saturation density that is one-fifth to one-sixth lower than that of Ni (111) and Pd (111). The means the phosphide phase may be able to better accommodate the otherwise very weakly coordinating nitrate ions and leads to 96% NH_3 selectivity. There are also reports of noble metal phosphides, being explored for other reactions. For instance, Furukawa et al. demonstrated that phosphidation of Ru to form Ru_2P improved activity 20-fold, compared to metallic Pt, Pd, and Rh for toluene hydrogenation (Fig. 15A and B).[224] Although the cost of precious metals (Fig. 15C) is very necessary to consider due to their scarcity, but not the only variable, we still need to consider other factors such as the source of P and the energy/material costs. The calculations (Fig. 15 D and E) demonstrated that the angles between phenyl ring and aromatic C−H bonds in Ru_2P were much larger than that in Ru surface, which led to the highly distorted and strongly adsorbed toluene on Ru_2P with an sp^3-like conformation, and thus enhanced the catalytic activity. Our group[225] reported a robust Ru phosphide (RuP) catalyst for propane dehydrogenation. The P element acted as a structural promoter to reduce Ru ensemble size which decreased the hydrogenolysis rate relative to Ru metal. Additionally, increasing P/Ru ratio resulted in lower energy for Ru valence orbitals, which weakened the metal-adsorbate energetics and decreased reactant coverages (Fig. 16), thus resulting in high propylene selectivity. Sulfur can also play a role in reducing ensembles size by blocking part of the active metal surface during steam reforming of methane. The as-obtained ensembles of free metal atoms are sufficient for the conversion of adsorbed methane with steam, but too small to allow for the normal nucleation of carbon whiskers and thus inhibit the formation of coke.[226] The catalytic behavior of amorphous metal borides for selective hydrogenation reactions is also well documented. The reports by Li et al. indicated that catalytic activity was linked to boron content[197] and was associated with the electronic influence of B on the active metal but also with the stable dispersion of small metal crystallites.[227]

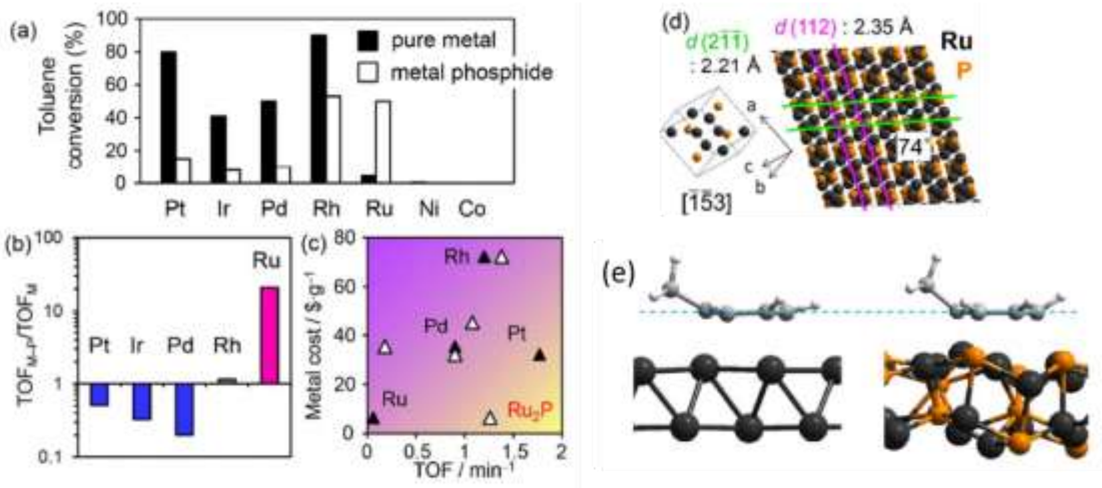

Fig. 15 (a) Toluene conversion and (b) change in TOF upon phosphidation of various SiO_2-supported transition metal and metal phosphides for toluene hydrogenation. (c) price of the main metal (2018) in the catalyst plotted against the TOF. (d) Crystal structures of Ru_2P viewed along [153] direction (left: single unit cell, right: periodic structure). Dihedral angle between (211) and (112) planes is shown (74°). (e) Side views of toluene adsorbed on Ru(0001) and (b) $Ru_2P(112)$ surfaces. Dotted line indicates the plane consisted of the aromatic ring. Reproduced with permission from ref 224. Copyright 2018 American Chemical Society.

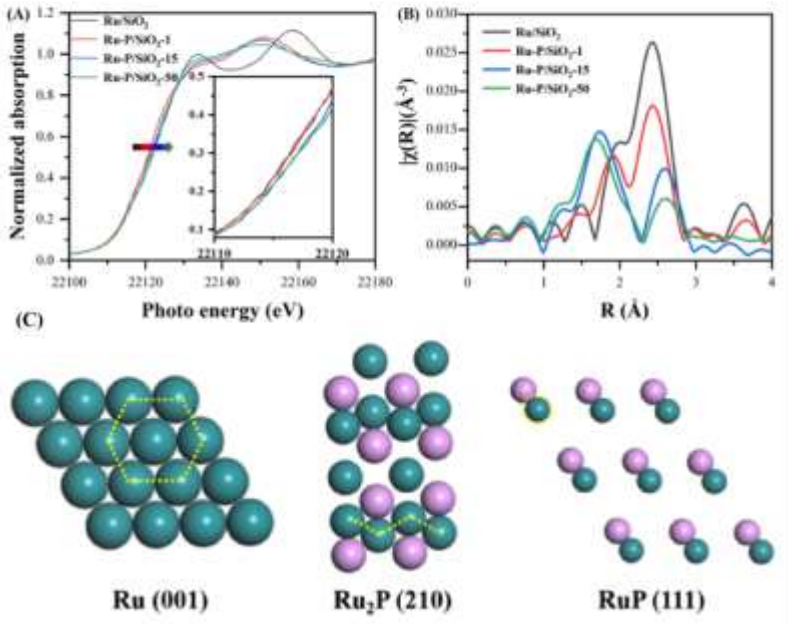

Fig. 16 (A) Ru K-edge (A) XANES spectra and (B) k^2-weighted magnitude of the Fourier transform of the EXAFS of Ru/SiO_2 and $Ru\text{-}P/SiO_2$ samples with different P:Ru atomic ratios (1, 15, and 50) (C) Ru ensemble size (dashed yellow line) for the most stable surface planes: (a) Ru (001), (b) Ru_2P (210), and (c) RuP (111). Ru atoms are shown in green, and P atoms are shown in purple. Reproduced with permission from ref 225. Copyright 2020 American Chemical Society.

In recent years, metal phosphides and sulfides have been explored for energy conversion applications. Liu et al. evaluated the activity of Ni_2P (001) in the hydrogen evolution reaction (HER)[142] and reported that the good electrocatalytic behavior obtained was attributable to an ensemble effect. More specifically, the active Ni sites were diluted by P atoms which could themselves act as proton-acceptor and hydride-acceptor centers which helped facilitate the HER. Later, Luo and coworkers[228] reported that FeP nanorod arrays supported on carbon cloth could act as a binder-free 3D hydrogen evolution cathode which possessed good activity and durability in acidic media but were also active in neutral and alkaline medium. Similarly, Co phosphide has been touted as a promising next-generation HER electrocatalyst with excellent catalytic properties as well as durability.[229] Nickel phosphide materials have also been explored as photothermal catalysts for the CO_2 hydrogenation reaction (note: photothermal indicates that the light source both activates the photocatalyst and provides photothermal heating). A $Ni_{12}P_5$ phase was identified as an excellent material since the underlying crystal structure leads to well-dispersed Ni nanoclusters that are spaced out by the P atoms (Fig. 17).[230] This sample also has the added benefit of harvesting light intensely across the entire range of solar spectra which leads to effective photothermal catalysis.. $Ni_{12}P_5$ provided a CO production rate of 960 ± 12 mmol g cat^{-1} h^{-1}, 100% selectivity and long-term stability. This concept was also extended to Co_2P analogs.[230]

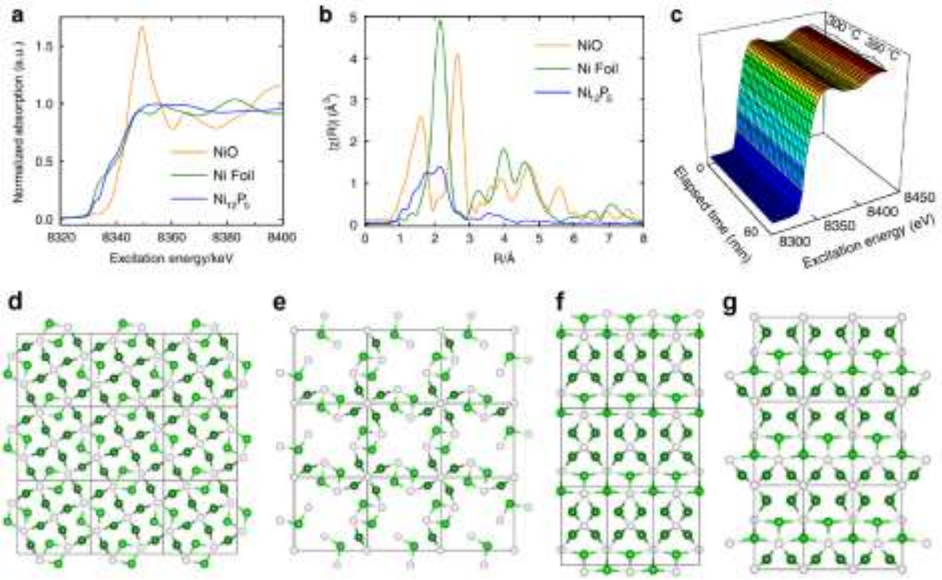

Fig. 17 XAS measurements. (a) Ni K-edge X-ray absorption near-edge structure (XANES) spectra, with Ni Foil and NiO powder included as references. (b) R-space spectra. (c) Time-resolved in situ XANES curves plotted in the simulated reaction condition (CO_2:H_2=5:1 gas flow, with a temperature of 300 °C or 350 °C). Surface crystal structure perspective of $Ni_{12}P_5$. (d, e) In the (001)

orientation. (f, g) in (010) orientation. Note the white spheres represent the P atoms, and Ni atom with two different coordination environments are depicted as dark green and light green spheres, respectively. Reproduced with permission from ref 230. Copyright 2020 Nature.

Due to attractive properties such as exceptional ionic conductivity and lower migration energy, metal sulfides have emerged as a novel class of materials for energy conversion. Lou et al.[231] converted 'onion-like' Co_4S_3 particles into unique $NiCo_2S_4$ hollow structured shells through a subsequent cation-exchange reaction with Ni^{2+} ions. Benefiting from the unique shell architecture and robust matrix, the as-prepared $NiCo_2S_4$ particles exhibit improved electrochemical performance as a battery-type electrode with outstanding cycling life and enhanced energy density. This group[232] also synthesized hierarchical $Fe_{1-x}S$-filled porous carbon nanowires/reduced graphene oxide. The material was efficient for sodium storage. Furthermore, $Cu_{1.8}S$ was suggested as a new anode material for Na-Ion batteries according.[233] Owing to the short ionic diffusion length, the $Cu_{1.8}S$ exhibited enhanced electrochemical properties and structural stability (related to strong Cu−S bonds and octahedral interstitial sites for Na^+ ions). Mo sulfide and main group metal sulfides (SnS microboxes) also display efficient sodium storage property with good capacity and excellent cycling stability.[234,235] Many binary (CdS, ZnS, MoS_2, SnS_2, Bi_2S_3, In_2S_3, Cu_2S, NiS/NiS_2, CoS_2), ternary ($ZnIn_2S_4$, $CdIn_2S_4$, $CuInS_2$, Cu_3SnS_4, and $CuGaS_2$), and quaternary (Cu_2ZnSnS_4) metal sulfide systems have also been considered as semiconductors for photocatalytic CO_2 reduction.[236] Very recently, Patir et al.[237] successfully synthesized Cu-based multinary sulfide (M:Cu_xS, M = Ni, Co, Mn or Zn) by a hot-injection method and used them as catalysts for the photocatalytic H_2 evolution under simulated sunlight irradiation. The Ni:Cu_xS nanorods were more active and provided more stable hydrogen evolution (4.0 mmol h^{-1} g^{-1}) than the other systems studied.

5. Conclusion and perspective for future studies/applications

In this review, recent progress in preparing and utilizing metal phosphides and metal sulfides have been summarized. Firstly, a diverse range of synthesis strategies have been described. Bulk phase methods can yield high purity phases which can help to elucidate structure-performance relationships since these materials are inherently easier to characterize than dispersed phases. Although, it is important to consider the role of surface chemistry which can be complex for these materials. Of course, for a heterogeneous catalyst it is preferable to have a highly dispersed active phase since this increases the number of active sites. Therefore, for a synthesis strategy to be considered effective for preparation of a heterogeneous catalyst it should ideally produce a single d-metal/p-block phase. It should also utilize both benign reagents (such as non-toxic hypophosphite, organophosphorus/sulfur compounds, or even S or P doped oxides) and synthesis conditions (i..e, low temperature). In this regard, solvothermal, precipitation and phosphination/sulfidation methods represent the most viable synthesis strategies, although template approaches are advantageous for fabricating metal-P block compounds with specific morphology.

Alteration of the d-metal/p-block element ratio changes both the geometry and electronic properties. In a metal-rich compound (i.e, Pd_3S or Pd_4S) the p-block element acts as a spacer which creates specific metal ensembles. However, as the ratio decreases you will gradually shift towards smaller ensembles and/or individual metal atoms. It is therefore desirable to have synthesis methods which allow for the facile alteration of the d-metal/p-block element ratio so that geometric changes to active sites can be systematically studied. In terms of electronic properties, there is typically a difference in electronegativity between the metal and the p-block compound. As such, there will be a degree of charge transfer from the metal to the non-metal which may create electron deficient metal atoms which are highly active. The degree of charge transfer will inevitably vary with the d-metal/p-block element stoichiometry. In other words, across a range of compositions you are likely to see a combination of effects which makes untangling electronic and geometric effects non-trivial. To aid with this, it is necessary to employ a combination of experimental and theoretical techniques with DOS, DFT calculations and XPS appearing especially helpful. The added advantage of DFT calculations being that consideration of surface relaxation effects can be included. It is also important to note these materials may undergo structural changes during operation under catalytic conditions. Therefore, ex-situ characterization should also be complimented by advanced *in situ* characterization methods such as XAS, XPS, XRD and AC-STEM to name a few. This helps to ensure that structure-performance relationships are based on an understanding of the catalyst under working conditions and not misconceptions derived from ex-situ measurements.

To date, metal phosphides and sulfides have been examined for a variety of applications, although many of these involve hydrogenation chemistry (i.e., HDS and HDN). This links to the metal atoms retaining metal character. Particularly noteworthy results have been achieved for the hydrogenation of unsaturated carbon-carbon bonds in both gas and liquid phases reactions. In these cases, metal sulfides have been shown to be especially selective but also highly active. Clear ensemble effects have been shown with both metal sulfides and phosphides offering uniform active sites that are simply not achievable in the absence of the p-block element. Whilst it can be argued that some degree of ensemble control is possible through alloying it will not necessarily be a uniform effect unless working with an intermetallic. Even then, the second metal may play a more pivotal role than the p-block element in the catalytic mechanism. Although, this remark is made with a degree of caution since literature includes examples where the p-block element may be actively involved in mechanistic steps.

Much more work is necessary to fully explore the concept of site-isolation in metal phosphides and sulfides, with special interest in alternative reactions (i.e., selective oxidations, C−H activations etc.) and the ongoing work exploring energy conversion where the interesting electronic properties of metal phosphides and sulfides seem especially important. The current state of literature reviewed in this work suggests that the rational design and synthesis of highly-efficient catalysts of practical use are achievable by using transition metal/p-block materials. Hence this topic is of widespread interest and importance.

AUTHOR INFORMATION

ORCID

Yanan Liu: 0000-0001-5125-0446

Alan J. McCue: 0000-0002-4404-6102

Dianqing Li: 0000-0001-6761-8946

Notes

The authors declare no competing financial interest.

Author contributions

Yanan Liu, as the first author, wrote the manuscript and prepared the figures/ references; Alan J. McCue provided ideas during the manuscript preparing stage and gave specific guidance during the writing and revision stages; Dianqing Li provided guidance on manuscript organization and content.

ACKNOWLEDGMENT

This work was supported by the project funded by National Natural Science Foundation of China, and the Fundamental Research Funds for the Central Universities (buctrc201921; JD2108).

REFERENCES

(1) Pelletier, D. A. J.; Basset, J. M. Catalysis by Design: Well-Defined Single-Site Heterogeneous Catalysts, *Acc. Chem. Res.* **2016**, *49*, 664−677.

(2) Zhang, L.; Zhou, M.; Wang, A.; Zhang, T. Selective Hydrogenation over Supported Metal Catalysts: From Nanoparticles to Single Atoms, *Chem. Rev.* **2020***, 120*, 683−733.

(3) Osswald, J.; Giedigkeit, R.; Jentoft, R. E.; Armbrüster, M.; Girgsdies, F.; Kovnir, K.; Ressler, T.; Grin, Y.; Schlögl R. Palladium–Gallium Intermetallic Compounds for the Selective Hydrogenation of Acetylene Part I: Preparation and Structural Investigation under Reaction Conditions, *J. Catal.* **2008***, 258*, 210–218.

(4) Li, J.; Li, X.; Zhai, H. J.; Wang, L. S. Au_{20}: A Tetrahedral Cluster. *Science* **2003**, *299*, 864–867.

(5) Valden, M.; Lai, X.; Goodman, D. W. Onset of Catalytic Activity of Gold Clusters on Titania with the Appearance of Nonmetallic Properties. *Science* **1998**, *281,* 1647–1650.

(6) Lopez, N.; Janssens, T. V. W.; Clausen, B. S.; Xu, Y.; Mavrikakis, M.; Bligaard, T.; Nørskov, J. K. On the Origin of the Catalytic Activity of Gold Nanoparticles for Low-Temperature CO Oxidation. *J. Catal.* **2004**, *223*, 232–235.

(7) Ji, S.; Chen, Y.; Wang, X.; Zhang, Z.; Wang, D.; Li, Y. D. Chemical Synthesis of Single Atomic Site Catalysts. *Chem. Rev.* **2020**, *120*, 11900–11955.

(8) Murzin, D. Y. Kinetic Analysis of Cluster Size Dependent Activity and Selectivity, *J. Catal.* **2010**, *276*, 85-91.

(9) King, M. E.; Personick, M. L. Iodide-Induced Differential Control of Metal Ion Reduction Rates: Synthesis of Terraced Palladium–Copper Nanoparticles with Dilute Bimetallic Surfaces. *J. Mater. Chem. A,* **2018**, *6*, 22179-22188.

(10) Chen, Y. J.; Ji, S. F.; Chen, C.; Peng, Q.; Wang, D. S.; Li, Y. D. Single-Atom Catalysts: Synthetic Strategies and Electrochemical Applications. *Joule,* **2018***, 2*, 1242.

(11) Yoon, B.; Häkkinen, H.; Landman, U.; Wörz, A. S.; Antonietti, J. M.; Abbet, S.; Judai, K.; Heiz, U. Charging Effects on Bonding and Catalyzed Oxidation of CO on Au_8 Clusters on MgO. *Science* **2005**, *307,* 403.

(12) Lu, J.; Aydin, C.; Browning, N. D.; Gates, B. C. Imaging Isolated Gold Atom Catalytic Sites in Zeolite NaY. *Angew. Chem. Int. Ed.* **2012***, 51,* 5842.

(13) Qiao, B.; Wang, A.; Yang, X.; Allard, L. F.; Jiang, Z.; Cui, Y.; Liu, J.; Li, J.; Zhang, T. Single-Atom Catalysis of CO Oxidation using Pt_1/FeO_x. *Nat. Chem.* **2011**, *3,* 634.

(14) Kwak, J. H.; Hu, J.; Mei, D.; Yi, C. W.; Kim, D. H.; Peden, C. H. F.; Allard, L. F. J. Szanyi, Coordinatively Unsaturated Al^{3+} Centers as Binding Sites for Active Catalyst Phases of Platinum on γ-Al_2O_3. *Science* **2009**, *325,* 1670.

(15) Yan, H.; Cheng, H.; Yi, H.; Lin, Y.; Yao, T.; Wang, C.; Li, J.; Wei, S.; Lu J. Single-Atom Pd_1/Graphene Catalyst Achieved by Atomic Layer Deposition: Remarkable Performance in Selective Hydrogenation of 1,3-Butadiene. *J. Am. Chem. Soc.* **2015,** *137,* 10484–10487.

(16) Flytzani-Stephanopoulos, M.; Gates, B. C. Atomically Dispersed Supported Metal Catalysts. *Annu. Rev. Chem. Biomol. Eng.* **2012,** *3,* 545–574.

(17) Wang, K.; Wang, X.; Liang X. Synthesis of High Metal Loading Single Atom Catalysts and Exploration of the Active Center Structure, *ChemCatChem* **2021**, *13*, 28-58.

(18) C. H. Choi, M. Kim, H. C. Kwon, S. J. Cho, S. Yun, H. T. Kim, K. J. Mayrhofer, H. Kim, M. Choi, Tuning Selectivity of Electrochemical Reactions by Atomically Dispersed Platinum Catalyst, *Nat. Commun.* **2016**, *7*, 10922.

(19) Y. Chen, S. Ji, Y. Wang, J. Dong, W. Chen, Z. Li, R. Shen, L. Zheng, Z. Zhuang, D. Wang, Y. Li, Isolated Single Iron Atoms Anchored on N-Doped Porous Carbon as an Efficient Electrocatalyst for the Oxygen Reduction Reaction, *Angew. Chem. Int. Ed.* **2017**, *56*, 6937-6941.

(20) Yang, X. F.; Wang, A. Q.; Qiao, B. T.; Li, J.; Liu, J. Y.; Zhang, T. Single-Atom Catalysts: A New Frontier in Heterogeneous Catalysis. *Acc. Chem. Res.* **2013**, *46*, 1740−1748.

(21) Zhang, L.; Wang, A.; Miller, J. T.; Liu, X.; Yang, X.; Wang, W.; Li, L.; Huang, Y.; Mou, C.-Y.; Zhang, T. Efficient and Durable Au Alloyed Pd Single-Atom Catalyst for the Ullmann Reaction of Aryl Chlorides in Water. *ACS Catal.* **2014,** *4,* 1546−1553.

(22) Kyriakou, G.; Boucher, M. B.; Jewell, A. D.; Lewis, E. A.; Lawton, T. J.; Baber, A. E.; Tierney, H. L.; Sykes, E. C. H.; Flytzani Stephanopoulos, M. Isolated Metal Atom Geometries as a Strategy for Selective Heterogeneous Hydrogenation. *Science* **2012,** *335,* 1209−1212.

(23) Carenco, S.; Portehault, D.; Boissière, C.; Mézailles, N.; Sanchez, C. Nanoscaled Metal Borides and Phosphides: Recent Developments and Perspectives. *Chem. Rev.* **2013**, *113*, 7981–8065.

(24) Anantharaj, S.; Ede, S. R.; Sakthikumar, K.; Karthick, K.; Mishra, S.; KunduRecent, S. Trends and Perspectives in Electrochemical Water Splitting with an Emphasis on Sulfide, Selenide, and Phosphide Catalysts of Fe, Co, and Ni: A Review. *ACS Catal.* **2016**, *6*, 8069−8097.

(25) Pei, Y.; Cheng, Y.; Chen, J. Y.; Smith, W.; Dong, P.; Ajayan, P. M.; Ye M. X.; Shen J. F. Recent Developments of Transition Metal Phosphides as Catalysts in the Energy Conversion Field. *J. Mater. Chem. A,* **2018**, *6*, 23220.

(26) Muetterties, E. L.; Sauer, J. C. Catalytic Properties of Metal Phosphides. Qualitative Assay of Catalytic Properties. I. *J Am Chem Soc.* **1974**, *96*, 3410–3415.

(27) Li W.; Dhandapani B.; Oyama, S. T. Molybdenum Phosphide: A Novel Catalyst for Hydrodenitrogenation. *Chem Lett*. **1998**, *27*, 207–210.

(28) Juan F. C.; Carlos G. R.; Christopher W. R.; Nathan S. L.; Raymond E. S. Characterization, and Properties of Metal Phosphide Catalysts for the Hydrogen-Evolution Reaction. *Chem. Mater*. **2016**, *28*, 6017−6044.
(29) Carenco, S.; Hu, Y.; Florea, I.; Ersen, O.; Boissiere, C.; Mezailles, N.; Sanchez, C. Metal-Dependent Interplay between Crystallization and Phosphorus Diffusion during the Synthesis of Metal Phosphide Nanoparticles, *Chem. Mater.* **2012**, *24*, 4134−4145.
(30) Hou, H.; Yang, Q.; Tan, C.; Ji, G.; Gu, B.; Xie, Y. One-pot Solution-phase Synthesis of Paramagnetic Co_2P Nanorods. *Chem. Lett.* **2004,** *33,* 1272–1273.
(31) Carenco, S.; Resa, I.; Le Goff, X.F.; Le Floch, P.; Mézailles, N. White Phosphorus as Single Source of "P" in the Synthesis of Nickel Phosphide. *Chem. Commun*. **2008**, 2568–2570.
(32) Carenco, S.; Le Goff, X. F.; Shi, J.; Roiban, L.; Ersen, O.; Boissiere, C.; Sanchez, C.; Mézailles, N. Magnetic Core−Shell Nanoparticles from Nanoscale-Induced Phase Segregation. *Chem. Mater*. **2011**, *23*, 2270–2277.
(33) Muthuswamy, E.; Kharel, P. R.; Lawes, G.; Brock, S. L. Control of Phase in Phosphide Nanoparticles Produced by Metal Nanoparticle Transformation: Fe_2P and FeP. *ACS Nano*. **2009**, *3*, 2383-2393.
(34) Zumbusch, M. Z. Uber die Strukturen des Uransubsulfids und der Subphosphide des Iridiums und Rhodiums. *Anorg. Allg. Chem*. **1940**, *243*, 322–329.
(35) De Trizio, L.; Figuerola, A.; Manna, L.; Genovese, A.; George, C.; Brescia, R.; Saghi, Z.; Simonutti, R.; Van Huis, M.; Falqui, A. Size-Tunable, Hexagonal Plate-like Cu_3P and Janus-like Cu–Cu_3P Nanocrystals. *ACS Nano.* **2012**, *6*, 32−41.
(36) Aitken, J. A.; Ganzha-Hazen, V. L.; Brock, S. L. Solvothermal Syntheses of Cu_3P via Reactions of Amorphous Red Phosphorus with a Variety of Copper Sources. *J. Solid State Chem.* **2005**, *178*, 970–975.
(37) Boyanov, S.; Bernardi, J.; Bekaert, E.; Ménétrier, M.; Doublet, M. L.; Monconduit, L. P-Redox Mechanism at the Origin of the High Lithium Storage in NiP_2-Based Batteries. *Chem. Mater*. **2009**, *21*, 298–308.
(38) Albani, D.; Karajovic, K.; Tata, B.; Li, Q.; Mitchell, S.; López N.; Pérez-Ramírez, J. Ensemble Design in Nickel Phosphide Catalysts for Alkyne Semi-Hydrogenation. *ChemCatChem.* **2019**, *11*, 457–464.
(39) Qian, X. F.; Zhang, X. M.; Wang, C.; Wang, W. Z.; Qian, Y. T. A New Way to Prepare Nanocrystalline Dinickel Phosphide. *Mater Res Bull*. **1998**, *33*, 669–672.
(40) Qian, X. F.; Xie, Y.; Qian, Y. T.; Zhang, X. M.; Wang, W. Z.; Yang, L. Organo-Thermal Preparation of Nanocrystalline Cobalt Phosphides. *Mater Sci Eng B*. **1997**, *49*, 135–137.
(41) Jarvis, R. F.; Jacubinas, R. M.; Kaner, R. B. Self-Propagating Metathesis Routes to Metastable Group 4 Phosphides. *Inorg Chem*. **2000**, *39*, 3243–3246.
(42) Gu, Y.; Gu, G. Y.; Guo F.; Qian, Y. T.; Zheng, H.; Yang, Z. A Solvothermal Synthesis of Ultra-FineIron Phosphide. *Mater Res Bull.* **2002**, *37,* 1101–1105.
(43) Wang, R.; Smith, K. J. Hydrodesulfurization of 4,6-Dimethyldibenzothiophene over High Surface Area Metal Phosphides. *Appl. Catal. A.* **2009**, *361*, 18–25.
(44) Whiffen, V. M. L.; Smith, K. J.; Straus, S. K. The influence of citric acid on the synthesis and activity of high surface area MoP for the hydrodeoxygenation of 4-methylphenol. *Appl. Catal. A.* **2012**, *419–420*,111–125.

(45) Yang, P.; Jiang, Z.; Ying, P.; Li, C. Effect of Surface Composition on the Catalytic Performance of Molybdenum Phosphide Catalysts in the Hydrogenation of Acetonitrile. *J. Catal.* **2008**, *253*, 66–73.

(46) Abu, I. I.; Smith, K. J. The Effect of Cobalt Addition to Bulk MoP and Ni_2P Catalysts for the Hydrodesulfurization of 4,6-Dimethyldibenzothiophene. *J. Catal.* **2006**, *241*, 356−366.

(47) Oyama, S. T. Novel Catalysts for Advanced Hydroprocessing: Transition Metal Phosphides. *J. Catal*. **2003**, *216*, 343−352.

(48) Oyama, S. T.; Gott, T.; Zhao, H.; Lee, Y. K. Transition Metal Phosphide Hydroprocessing Catalysts: A Review. *Catal. Today*. **2009**, *143*, 94-107.

(49) Kibsgaard J.; Tsai C.; Chan K.; Benck J. D.; Nørskov J. K.; Abild-Pedersen F.; Jaramillo T. F. Designing an Improved Transition Metal Phosphide Catalyst for Hydrogen Evolution using Experimental and Theoretical Trends. *Energy Environ. Sci.* **2015**, *8*, 3022.

(50) Guan, Q.; Zhang, M.; Tao, K. Alternative Synthesis of Bulk and Supported Nickel Phosphide from the Thermal Decomposition of Hypophosphites. *J. Catal.* **2009**, *263*, 1–3.

(51) Tian, L.; Yan, X.; Chen, X. Electrochemical Activity of Iron Phosphide Nanoparticles in Hydrogen Evolution Reaction. *ACS Catal*. **2016**, *6*, 5441−5448.

(52) Liu, K.; Zhang, C.; Sun, Y.; Zhang, G.; Shen, X.; Zou, F.; Zhang, H.; Wu, Z.; Wegener, E. C.; Taubert, C. J.; Miller, J. T.; Peng, Z.; Zhu, Yu. High-Performance Transition Metal Phosphide Alloy Catalyst for Oxygen Evolution Reaction. *ACS Nano*. **2018**, *12*, 158−167.

(53) Perera, S. C.; Tsoi, G.; Wenger, L. E.; Brock, S. L. Synthesis of MnP Nanocrystals by Treatment of Metal Carbonyl Complexes with Phosphines: A New, Versatile Route to Nanoscale Transition Metal Phosphides. *J. Am. Chem. Soc*. **2003**, 125, 13960–13961.

(54) Perera, S. C.; Fodor, P. S.; Tsoi, G. M.; Wenger, L. E.; Brock, S. L. Application of De-silylation Strategies to the Preparation of Transition Metal Pnictide Nanocrystals: The Case of FeP. *Chem Mater*. **2003**, 15, 4034–4038.

(55) Chiang, R.; Chiang, R. Formation of Hollow Ni_2P Nanoparticles Based on the Nanoscale Kirkendall Effect. *Inorg. Chem.* **2007**, *46*, 369.

(56) Muthuswamy, E.; Savithra, G. H. L.; Brock, S. L. Synthetic Levers Enabling Independent Control of Phase, Size, and Morphology in Nickel Phosphide Nanoparticles. *ACS Nano*. **2011**, *5*, 2402−2411.

(57) Roel P.; Mark E. B. Metal Phosphides: Preparation, Characterization and Catalytic Reactivity. *Catal Lett*. **2012**, 142 (12), 1413-1436.

(58) Wang, T.; Wang, C.; Jin, Y.; Sviripa, A.; Liang, J.; Han, J.; Huang, Y.; Li, Q.; Wu, G. Amorphous Co–Fe–P Nanospheres for Efficient Water Oxidation. *J. Mater. Chem. A*. **2017**, *5*, 25378–25384.

(59) Khanna, P. K.; Jun, K.-W.; Hong, K. B.; Baeg, J.-O.; Mehrotra, G. K. Synthesis of Indium Phosphide Nanoparticles via Catalytic Cleavage of Phosphorus Carbon Bond in n-Trioctylphosphine by Indium. *Mater. Chem. Phys*. **2005**, *92*, 54.

(60) Khanna, P. K.; Singh, N.; More, P. Synthesis and Band-Gap Photoluminescence from Cadmium Phosphide Nanoparticles. *Curr. Appl. Phys*. **2010**, *10*, 84.

(61) Carenco, S.; Liu, Z.; Salmeron, M. The Birth of Nickel Phosphide Catalysts: Monitoring Phosphorus Insertion into Nickel. *ChemCatChem*. **2017**, *9*, 2318-2323.

(62) Popczun E. J.; McKone J. R.; Read C. G. et al. Nanostructured Nickel Phosphide as An Electrocatalyst for the Hydrogen Evolution Reaction. *J. Am. Chem. Soc*. **2013**, *135(25)*, 9267-9270.

(63) Duttmann, A.; Bottke, P.; Plaggenborg, T.; Gutsche, C.; Parisi, J.; Knipper, M.; Kolny-Olesiak, J. Converting Bimetallic M (M=Ni, Co, or Fe)–Sn Nanoparticles into Phosphides: A General Strategy for the Synthesis of Ternary Metal Phosphide Nanocrystals. *Nanoscale Adv*. **2019**, *1*, 2663.
(64) Huang, Z.; Chen, Z.; Chen, Z.; Lv, C.; Mark G. H.; Zhang, C. Cobalt Phosphide Nanorods as an Efficient Electrocatalyst for the Hydrogen Evolution Reaction. *Nano Energy*. **2014**, *9*, 373–382.
(65) Mundy, M. E.; Ung, D.; Lai, N. L.; Jahrman, E. P.; Seidler, G. T.; Cossairt, B. M. Aminophosphines as Versatile Precursors for the Synthesis of Metal Phosphide Nanocrystals. *Chem. Mater*. **2018**, *30*, 5373−5379.
(66) Sung, J.; Goedde, D. M.; Girolami, G. S.; Abelson, J. R. Remote-Plasma Chemical Vapor Deposition of Conformal ZrB_2 Films at Low Temperature: A Promising Diffusion Barrier for Ultralarge Scale Integrated Electronics. *J. Appl. Phys*. **2002**, *91*, 3904.
(67) Liu, Y. N.; McCue, A. J.; Feng, J. T.; Guan, S. L.; Li, D. Q.; Anderson, J. A. Evolution of Palladium Sulfide Phases during Thermal Treatments and Consequences for Acetylene Hydrogenation. *J. Catal*. **2018**, *364*, 204–215.
(68) Chen, C. J. Chiang, R. K. Sulfidation of Rock-Salt-Type Transition Metal Oxide Nanoparticles as an Example of a Solid State Reaction in Colloidal Nanoparticles. *Dalton Trans*. **2011**, *40*, 880–885.
(69) Levard, C.; Reinsch, B. C.; Michel, F. M.; Oumahi, C.; Lowry, G. V.; Brown Jr, G. E. Sulfidation Processes of PVP-Coated Siler Nanoparticles in Aqueous Aolution: Impact on Dissolution Rate. *Environ. Sci. Technol*. **2011**, *45*, 5260–5266.
(70) Kuang, P.; Tong, T.; Fan, K.; Yu, J. In Situ Fabrication of Ni−Mo Bimetal Sulfide Hybrid as an Efficient Electrocatalyst for Hydrogen Evolution over a Wide pH Range. *ACS Catal*. **2017**, *7*, 6179−6187.
(71) Zhang, L.; Zhou, L.; Wu, H. B.; Xu, R.; Lou, X. W. Unusual Formation of Single-Crystal Manganese Sulfide Microboxes Co-Mediated by the Cubic Crystal Structure and Shape. *Angew. Chem., Int. Ed*. **2012**, *51*, 7267–7270.
(72) Cummins, D. R.; Russell, H. B.; Jasinski, J. B.; Menon, M.; Sunkara, M. K. Iron Sulfide (FeS) Nanotubes using Sulfurization of Hematite Nanowires. *Nano Lett*. **2013**, *13*, 2423–2430.
(73) Kung, C. W.; Chen, H. W.; Lin, C. Y.; Huang, K. C.; Vittal, R.; Ho, K. C. CoS Acicular Nanorod Arrays for the Counter Electrode of an Efficient Dye-Sensitized Solar Cell. *ACS Nano*. **2012**, *6*, 7016–7025.
(74) Chen, H. W.; Kung, C. W.; Tseng, C.-M.; Wei, T.-C.; Sakai, N.; Morita, S.; Ikegami, M.; Miyasaka, T.; Ho, K. C. Plastic Based Dye-Sensitized Solar Cells using Co_9S_8 Acicular Nanotube Arrays as the Counter Electrode. *J. Mater. Chem. A*. **2013**, *1*, 13759–13768.
(75) Choi, S. H.; Kang, Y. C. Synthesis for Yolk-Shell-Structured Metal Sulfide Powders with Excellent Electrochemical Performances for Lithiu-Ion Batteries. *Small*. **2014**, *10*, 474–478.
(76) Dutta, A. K.; Maji, S. K.; Srivastava, D. N. A. Mondal, P. Biswas, P. Paul.; Adhikary, B. Synthesis of FeS and FeSe Nanoparticles from a Single Source Precursor: A Study of Their Photocatalytic Activity, Peroxidase-Like Behavior, and Electrochemical Sensing of H_2O_2. *ACS Appl. Mater. Interfaces*. **2012**, *4*, 1919–1927.
(77) She, H.; Sun, Y.; Li, S.; Huang, J.; Wang, L.; Zhu, G.; Wang, Q. Synthesis of Non-Noble Metal Nickel Doped Sulfide Solid Solution for Improved Photocatalytic Performance. *Appl. Catal. B: Environ*. **2019**, 245, 439–447.

(78) Xu, C.; Zeng, Y.; Rui, X. H.; Xiao, N.; J. Zhu, X.; Zhang, W. Y.; Chen, J.; Liu, W. L.; Tan, H. T.; Hng, H. H.; and Yan, Q. Y. Controlled Soft-Template Synthesis of Ultrathin C@FeS Nanosheets with High-Li-Storage Performance. *ACS Nano*. **2012**, *6*, 4713–4721.

(79) Lai, C. H.; Huang, K. W.; Cheng, J. H.; Lee, C. Y.; Hwang B. J.; Chen, L. J. Direct Growth of High-Rate Capability and High Capacity Copper Sulfide nanowire Array Cathodes for Lithium-Ion Batteries. *J. Mater. Chem*. **2010**, *20*, 6638–6645.

(80) Cai, R.; Chen, J.; Zhu, J. X.; Xu, C.; Zhang, W. Y.; Zhang, C. M.; Shi, W. H.; Tan, H. T.; Yang, D.; Hng, H. H.; Lim, T. M.; Yan, Q. Y. Synthesis of Cu_xS/Cu Nanotubes and Their Lithium Storage Properties. *J. Phys. Chem. C*. **2012**, *116*, 12468–12474.

(81) Ding L; Zheng M.; Wang A.; Zhang T. A Novel Route to the Preparation of Carbon Supported Nickel Phosphide Catalysts by a Microwave Heating Process. *Catal Lett*. **2010**, *135*, 305–311.

(82) Yu, F.; Zhou, H.; Huang, Y.; Sun, J.; Qin, F.; Bao, J.; Goddard, W. A.; Chen, S.; Ren, Z. High-Performance Bifunctional Porous Non-Noble Metal Phosphide Catalyst for Overall Water Splitting. High-Performance Bifunctional Porous Non-Noble Metal Phosphide Catalyst for Overall Water Splitting. *Nat. Commun*. **2018**, *9*, 2551.

(83) Xiong, D.; Wang, X.; Li, W.; Liu, L. Facile Synthesis of Iron Phosphide Nanorods for Efficient and Durable Electrochemical Oxygen Evolution. *Chem. Commun*. **2016**, *52(56)*: 8711-8714.

(84) Gong, S.; Liu, L.; He, H.; Cui, Q. Dibenzothiophene Hydrodesulfurization over MoP/SiO_2 Catalyst Prepared with Sol-Gel Method. *Korean J. Chem. Eng*. **2010**, *27*, 1419.

(85) Teixeira da Silva V.; Sousa L. A.; Amorim R. M.; Andrini L.; Figueroa S. J. A.; Requejo F. G.; Vincentini F. C. Lowering the Synthesis Temperature of Ni_2P/SiO_2 by Palladium Addition. *J. Catal.* **2011**, *279*, 88–102.

(86) Lin, J.; Feng, F.; Jiang, D.; Guan, Z.; Li, X. Highly Active and Stable Ni_2P/SiO_2 Catalyst for Hydrogenation of C9 Petroleum Resin, China Petroleum Processing and Petrochemical Technology. *Catalyst Research*. **2016**, *18 (1)*, 36-43.

(87) Shu, Y.; Lee, Y.; Oyama, S. Structure-Sensitivity of Hydrodesulfurization of 4,6-Dimethyldibenzothiophene over Silica-Supported Nickel Phosphide Catalysts. *J. Catal*. **2005**, *236*, 112-121.

(88) Cho, K. S.; Lee, Y. K. XAFS Studies on Highly Dispersed Ni_2P/SiO_2 Catalysts for Hydrodesulfurization of 4,6-Dimethyldibenzothiophene. *Nucl. Instrum. Methods Phys. Res., Sect. A*. **2010**, *621*, 690.

(89) Sun F.; Wu W.; Wu Z.; Guo J.; Wei Z.; Yang Y.; Jiang Z.; Tian F.; Li C. Dibenzothiophene Hydrodesulfurization Activity and Surface Sites of Silica-Supported MoP, Ni_2P, and Ni-Mo-P catalysts. *J. Catal.* **2004**, *228*, 298–310.

(90) Wang, H.; Shu, Y.; Wang, A.; Wang, J.; Zheng, M.; Wang, X.; Zhang, T. One-Pot Synthesis and Characterization of Metal Phosphide-Doped Carbon Xerogels. *Carbon*. **2008**, *46*, 2076.

(91) Chen J.; Chen Y.; Yang Q.; Li K.; Yao, C. An Approach to Preparing Highly Dispersed Ni_2P/SiO_2 Catalyst. *Catal Commun*. **2010**, *11*, 571–575.

(92) Clark, P. A.; Oyama, S. T. Alumina-Supported Molybdenum Phosphide Hydroprocessing Catalysts, *J. Catal.,* **2003***, 218*, 78-87.

(93) Zuzaniuk, V.; Prins, R. Synthesis and Characterization of Silica-Supported Transition-Metal Phosphides as HDN Catalysts, *J. Catal.,* **2003***, 219*, 85-96.

(94) Sawhill, S. J.; Layman, K. A.; Van, W. D. R.; Engelhard, M. H.; Wang, C.; Bussell, M. E. Thiophene Hydrodesulfurization over Nickel Phosphide Catalysts: Effect of the Precursor Composition and Support. *J. Catal.* **2005**, *231*, 300–313

(95) Yang, S.; Prins, R. New Synthesis Method for Nickel Phosphide Hydrotreating Catalysts. *Chem. Commun.* **2005**, *33*, 4178–4180.

(96) Yang S.; Liang C.; Prins R. A Novel Approach to Synthesizing Highly Active Ni_2P/SiO_2 Hydrotreating Catalysts. *J. Catal*. **2006**, *237*, 118–130.

(97) Bui, P.; Cecilia, J. A.; Oyama, S. T.; Takagaki, A.; I-Molina, A.; Zhao, H.; Li, D.; R-Castellon E. Lopez, A. J. Studies of the Synthesis of Transition Metal Phosphides and Their Activity in the Hydrodeoxygenation of a Biofuel Model Compound. *J. Catal*. **2012**, *294*, 184-198.

(98) Cecilia, J. A.; Infantes-Molina, A.; Rodríguez-Castellón, E.; Jiménez-López, A. A Novel Method for Preparing an Active Nickel Phosphide Catalyst for HDS of Dibenzothiophene. *J. Catal.* **2009***, 263*, 4-15.

(99) Liu, Y. N.; McCue, A. J.; Miao, C. L.; Feng, J. T.; Li, D. Q.; Anderson, J. A. Palladium Phosphide Nanoparticles as Highly Selective Catalysts for the Selective Hydrogenation of Acetylene. *J. Catal*. **2018**, *364*, 406–414.

(100) Bowker, R. H.; Smith, M. C.; Pease, M. L.; Slenkamp, K. M.; Kovarik L.; Bussel M. E. Synthesis and Hydrodeoxygenation Properties of Ruthenium Phosphide Catalysts. *ACS Catal*. **2011**, *1,* 917–922.

(101) Jiang, P.; Liu, Q.; Sun, X. NiP_2 Nanosheet Arrays Supported on Carbon Cloth: An Efficient 3D Hydrogen Evolution Cathode in Both Acidic and Alkaline Solutions. *Nanoscale.* **2014**, *6*, 13440−13445.

(102) Shi, Y.; Xu, Y.; Zhuo, S.; Zhang, J.; Zhang, B. Ni_2P Nanosheets/Ni Foam Composite Electrode for Long-Lived and pH-Tolerable Electrochemical Hydrogen Generation. *ACS Appl. Mater. Interfaces* **2015**, *7*, 2376−2384.

(103) Ryu, J.; Jung, N.; Jang, J. H.; Kim, H. J.; Yoo, S. J. In Situ Transformation of Hydrogen-Evolving CoP Nanoparticles: Toward Efficient Oxygen Evolution Catalysts Bearing Dispersed Morphologies with Co-oxo/hydroxo Molecular Units. *ACS Catal.* **2015**, *5*, 4066−4074.

(104) Wang, C.; Jiang, J.; Zhou, X.; Wang, W.; Zuo, J.; Yang, Q. Alternative Synthesis of Cobalt Monophosphide@C Core–Shell Nanocables for Electrochemical Hydrogen Production. *J. Power Sources* **2015**, *286*, 464−469.

(105) Pan, Y.; Lin, Y.; Chen, Y.; Liu, Y.; Liu, C. Cobalt Phosphide-Based Electrocatalysts: Synthesis and Phase Catalytic Activity Comparison for Hydrogen Evolution. *J. Mater. Chem. A*. **2016**, *4*, 4745.

(106) Zhao, M.; Abe, K.; Yamaura, S.; Yamamoto, Y.; Asao, N. Fabrication of Pd-Ni−P Metallic Glass Nanoparticles and Their Application as Highly Durable Catalysts in Methanol Electro Oxidation. *Chem. Mater*. **2014**, *26*, 1056−1061.

(107) Schaefer, Z. L.; Ke, X.; Schiffer, P.; Schaak, R. E. Direct Solution Synthesis, Reaction Pathway Studies, and Structural Characterization of Crystalline Ni_3B Nanoparticles. *J. Phys. Chem. C* **2008**, *112*, 19846.

(108) Bara, C.; Lamic-Humblot, A. F.; Fonda, E.; Gay, A. S.; Taleb, A. L.; Devers, E.; Digne, M.; Pirngruber G. D. Carrier, X. Surface-Dependent Sulfidation and Orientation of MoS_2 Slabs on Alumina-Supported Model Hydrodesulfurization Catalysts. *J. Catal*. **2016**, *344*, 591–605.

(109) Xu, W.; Ni, J.; Zhang, Q.; Feng, F.; Xiang, Y.; Li, X. Tailoring Supported Palladium Sulfide Catalysts Through H_2-Assisted Sulfidation with H_2S. *J. Mater. Chem. A*. **2013**, *1*, 12811.

(110) Liu, D.; Lu, Q.; Luo, Y.; Sun, X.; Asiri, A. M. $NiCo_2S_4$ Nanowires Array as an Efficient Bifunctional Electrocatalyst for Full Water Splitting with Superior Activity. *Nanoscale* **2015**, *7*, 15122−15126

(111) Beltran-Huarac, J.; Resto, O.; Carpena-Nunez, J.; Jadwisienczak, W. M.; Fonseca, L. F.; Weiner, B. R.; Morell, G. Single-Crystal γ-MnS Nanowires Conformally Coated with Carbon. *ACS Appl. Mater. Interfaces*, **2014**, *6*, 1180–1186.

(112) Ganesan, P.; Prabu, M.; Sanetuntikul, J.; Shanmugam, S. Cobalt Sulfide Nanoparticles Grown on Nitrogen and Sulfur Codoped Graphene Oxide: An Efficient Electrocatalyst for Oxygen Reduction and Evolution Reactions. *ACS Catal.* **2015**, *5*, 3625−3637.

(113) Whitham, P. J.; Strommen, D. P.; Lundell, S.; Lau L. D.; Rodriguez, R. GeS_2 and $GeSe_2$ PECVD from $GeCl_4$ and Various Chalcogenide Precursors. *Plasma Chem. Plasma Process.,* **2014**, *34*, 755–766.
(114) Lim, Y. R.; Song, W.; Han, J. K.; Lee, Y. B.; Kim, S. J.; Myung, S.; Lee, S. S.; An, K. S.; Choi, C. J.; Lim, J. Wafer-Scale, Homogeneous MoS_2 Layers on Plastic Substrates for Flexible Visible-Light Photodetectors. *Adv. Mater.,* **2016**, *28*, 5025–5030.
(115) Moody, M. J.; Henning, A.; Jurca, T.; Shang, J. Y.; Bergeron, H.; Balla, I.; Olding, J. N.; Weiss, E. A.; Hersam, M. C.; Lohr, T. L. Atomic Layer Deposition of Molybdenum Oxides with Tunable Stoichiometry Enables Controllable Doping of MoS_2. *Chem. Mater.*, **2018**, *30*, 3628–3632.
(116) Kim, H. J.; Yang, S.; Kim, H.; Moon, J. Y.; Park, K.; Park, Y. J.; Kwon, J. Y. Enhanced Electrical and Optical Properties of Single-Layered MoS_2 by Incorporation of Aluminum. *Nano. Res.*, **2018**, *11*, 731–740.
(117) Su, S.; Zhou, Q.; Zeng, Z.; Hu, D.; Wang, X.; Jin, M.; Gao, X.; Notzel, R.; Zhou, G.; Zhang, Z. Ultrathin Alumina Mask-Assisted Nanopore Patterning on Monolayer MoS_2 for Highly Catalytic Efficiency in Hydrogen Evolution Reaction. *ACS Appl. Mater. Interfaces*, **2018**, *10*, 8026–8035.
(118) Aslan, E.; Akin, I.; Patir, I. H. Highly Active Cobalt Sulfide/Carbon Nanotube Catalyst for Hydrogen Evolution at Soft Interfaces. *Chem. Eur. J.* **2016**, *22*, 5342−5349.
(119) Wang, H.; Li, Z.; Li, G.; Peng, F.; Yu, H. Co_3S_4/NCNTs: A Catalyst for Oxygen Evolution Reaction. *Catal. Today* **2015**, *245*, 74−78.
(120) Wang, D. Y.; Gong, M.; Chou, H. L.; Pan, C. J.; Chen, H. A.; Wu, Y.; Lin, M. C.; Guan, M.; Yang, J.; Chen, C. W.; Wang, Y. L.; Hwang, B. J.; Chen, C. C.; Dai, H. Highly Active and Stable Hybrid Catalyst of Cobalt-Doped FeS_2 Nanosheets–Carbon Nanotubes for Hydrogen Evolution Reaction. *J. Am. Chem. Soc.* **2015**, *137*, 1587−1592.
(121) Miao, J.; Xiao, F.-X.; Yang, H. B.; Khoo, S. Y.; Chen, J.; Fan, Z.; Hsu, Y.-Y.; Chen, H. M.; Zhang, H.; Liu, B. Hierarchical Ni-Mo-S Nanosheets on Carbon Fibercloth: A Flexible Electrode for Efficient Hydrogengeneration in Neutral Electrolyte. *Sci. Adv.* **2015**, *1*, 1500259.
(122) Bachiller-Baeza, B.; Iglesias-Juez, A.; Castillejos-López, E.; Guerrero-Ruiz, A.; Di Michiel, M.; Fernández-García, M.; Rodríguez-Ramos, I. Detecting the Genesis of a High-Performance Carbon-Supported Pd Sulfide Nanophase and Its Evolution in the Hydrogenation of Butadiene. *ACS Catal*. **2015**, **5**, 5235–5241.
(123) Li, D.; Maiti, U.; Lim, J.; Choi, D.; Lee, W.; Oh, Y.; Lee, G.; Kim, S. Molybdenum Sulfide/N-Doped CNT Forest Hybrid Catalysts for High-Performance Hydrogen Evolution Reaction. *Nano Lett*. **2014**, *14*, 1228−1233.
(124) Wang, J.; Liu, D.; Huang, H.; Yang, N.; Yu, B.; Wen, M.; Wang, X.; Chu, P. K.; Yu, X. In-Plane Black Phosphorus/Dicobalt Phosphide Heterostructure for Efficient Electrocatalysis. *Angew. Chem*. **2018**, *130*, 2630–2634.
(125) Morales, M.; Guerrero-Ruiz, A.; Castillejos, E.; Asedegbega-Nieto, E.; Rodríguez Ramos, I. Taking Advantage of Sulfur Impurities Present in Commercial Carbon Nanofibers to Generate Selective Palladium Catalysts. *Carbon*, **2020**, *157*, 120.
(126) Zhang, Y.; Wen, X.; Shi, Y.; Yue, R.; Bai, L.; Liu, Q.; Ba, X. Sulfur-Containing Polymer As a Platform for Synthesis of Size Controlled Pd Nanoparticles for Selective Semihydrogenation of Alkynes. *Ind. Eng. Chem. Res*. **2019**, *58*, 1142−1149.
(127) Kargar, F.; Coleman, E. A.; Ghosh, S.; Lee, J.; Gomez M. J.; Liu Y.; Magana, A.; Barani, Z.; Mohammadzadeh, A.; Debnath, B.; Wilson, R. B.; Lake, R. K.; Balandin, A. A. Phonon and Thermal Properties of Quasi-Two-Dimensional $FePS_3$ and $MnPS_3$ Antiferromagnetic Semiconductors. *ACS Nano* **2020**, *14(2),* 2424–2435.
(128) Zhu, W.; Gan, W.; Muhammad, Z.; Wang, C.; Wu, C.; Liu, H.; Liu, D.; Zhang, K.; He, Q.; Jiang, H.; Zheng, X.; Sun, Z.; Chen, S.; Song L. Exfoliation of Ultrathin $FePS_3$ Layers as a Promising Electrocatalyst for the Oxygen Evolution Reaction. *Chem. Commun.*, **2018**, *54*, 4481-4484.
(129) Dai, Z.; Geng, H.; Wang, J.; Luo, Y.; Li, B.; Zong, Y.; Yang, J.; Guo, Y. G.; Zheng, Y.; Wang, X.; Yan, Q. Hexagonal-Phase Cobalt Monophosphosulfide for Highly Efficient Overall Water Splitting. *ACS Nano*, **2017**, *11*, 11031–11040.

(130) Elshahawy, A. M.; Guan C.; Li X.; Zhang H.; Hu Y.; Wu H.; Pennycook S. J.; Wang J. Sulfur-Doped Cobalt Phosphide Nanotube Arrays for Highly Stable Hybrid Super Capacitor. *Nano Energy*. **2017**, *39*, 162–171.

(131) Xin, Y.; Kan, X.; Gan, L.; Zhang, Z. Heterogeneous Bimetallic Phosphide/Sulfide Nanocomposite for Efficient Solar-Energy-Driven Overall Water Splitting. *ACS Nano*. **2017**, *11*, 10303-10312.

(132) Kucernak, A. R. J.; Sundaram, V. N. N. Nickel phosphide: the effect of phosphorus content on hydrogen evolution activity and corrosion resistance in acidic medium, *J. Mater. Chem. A* **2014**, *2*, 17435−17445.

(133) Yang, Z.; Liu, L.; Wang, X.; Yang, S.; Su, X. Stability and Electronic Structure of the Co–P Compounds from First-Principle Calculations. *J. Alloys Compd*. **2011**, *509*, 165.

(134) Grosvenor, A. P.; Wik, S. D.; Cavell, R. G.; Mar, A. Examination of the Bonding in Binary Transition-Metal Monophosphides MP (M = Cr, Mn, Fe, Co) by X-Ray Photoelectron Spectroscopy. *Inorg. Chem*. **2005**, *44*, 8988.

(135) Blanchard, P. E. R.; Grosvenor, A. P.; Cavell, R. G.; Mar, A. X-ray Photoelectron and Absorption Spectroscopy of Metal-Rich Phosphides M_2P and M_3P (M=Cr-Ni). *Chem. Mater*. **2008**, *20*, 7081.

(136) Zintl, E. Intermetallische Verbindungen. *Angew. Chem*. **1939**, *52*, 1.

(137) Klemm, W. Metalloids and their Compounds with the Alkali Metals. Proc. *Chem. Soc.* **1958**, *329*.

(138) Hafner, J.; Tegze, M.; Becker, C. Amorphous Magnetism in Fe-B alloys: First-Principles Spin-Polarized Electronic-Structure Calculations. *Phys. Rev. B*. **1994**, *49*, 285.

(139) Von Schnering, H. G.; Hoenle, W. Chemistry and Structural Chemistry of Phosphides and Polyphosphides. 48. Bridging Chasms with Polyphosphides. *Chem. Rev.* **1988**, *88*, 243.

(140) Alexandera A.; Hargreaves, J. Alternative Catalytic Materials: Carbides, Nitrides, Phosphides and Amorphous Boron Alloys. *Chem. Soc. Rev*. **2010**, *39*, 4388–4401.

(141) Kanama, D.; Oyama, S.; Otani, S.; Cox, D. Photoemission and LEED Characterization of Ni_2P (0001). *Surf. Sci*. **2004**, *552*, 8.

(142) Liu, P.; Rodriguez, J. A. Catalysts for Hydrogen Evolution from the [NiFe] Hydrogenase to the Ni_2P(001) Surface: The Importance of Ensemble Effect. *J. Am. Chem. Soc*. **2005**, *127*, 14871−14878.

(143) Feng, Z.; Liang, C.; Wu, W.; Wu, Z.; van Santen, R. A.; Li, C. Carbon Monoxide Adsorption on Molybdenum Phosphides: Fourier Transform Infrared Spectroscopic and Density Functional Theory Studies. *J. Phys. Chem. B,* **2003**, *107*, 13698–13702.

(144) Shi, Y.; Zhang, B. Recent Advances in Transition Metal Phosphide Nanomaterials: Synthesis and Applications in Hydrogen Evolution Reaction. *Chem. Soc. Rev.* **2016**, *45*, 1529−1541.

(145) Rui, X.; Tan H.; Yan, Q. Nanostructured Metal Sulfides for Energy Storage. *Nanoscale*, **2014**, *6*, 9889–9924.

(146) Wang, C. Y.; Fang, Z.; Fan, F.; Dong, X. N.; Peng, Y.; Hao S. H.; Long, L. Y. Facile Synthesis of Size-Tunable $Cu_{39}S_{28}$ Micro/Nano-Crystals and Small-Sized Configuration Enhanced Visible-Light Photocatalytic Activity. *CrystEngComm*. **2013**, *15*, 5792–5798.

(147) Casaca, A.; Lopes, E. B.; Goncalves A. P.; Almeida, M. Electrical Transport Properties of CuS Single Crystals. *J. Phys.: Condens. Matter*. **2012**, *24*, 015701.

(148) Xu, Q.; Huang, B.; Zhao, Y. F.; Yan, Y. F.; Nou R.; Wei, S. H. Crystal and Electronic Structures of Cu_xS Solar Cell Absorbers. *Appl. Phys. Lett.,* **2012**, *100*, 061906.

(149) Wang, S. H.; Yang, S. H.; Dai Z. R.; Wang, Z. L. The Crystal Structure and Growth Direction of Cu_2S Nanowire Arrays Fabricated on a Copper Surface. *Phys. Chem. Chem. Phys*. **2001**, *3*, 3750–3753.
(150) Kullerud G.; Yund, R. A. The Ni-S System and Related Minerals. *J. Petrol*. **1962**, *3*, 126–175.
(151) Yu S. H.; Yoshimura, M. Fabrication of Powders and Thin Films of Various Nickel Sulfides by Soft Solution-Processing Routes. *Adv. Funct. Mater*. **2002**, *12*, 277–285.
(152) Idris, N. H.; Rahman, M. M.; Chou, S. L.; Wang, J. Z.; Wexler D.; Liu, H. K. Rapid Synthesis of Binary α-NiS–β-NiS by Microwave Autoclave for Rechargeable Lithium Batteries. *Electrochimica. Acta*. **2011**, *58*, 456–462.
(153) Ma, X.; Zhang, W.; Deng, Y.; Zhong, C.; Hu, W.; Han, X. Phase and Composition Controlled Synthesis of Cobalt Sulfide Hollow Nanospheres for Electrocatalytic Water Splitting. *Nanoscale*. **2018**, *10*, 4816–4824.
(154) Wang, Z.; Pan, L.; Hu H.; Zhao, S. Co_9S_8 Nanotubes Synthesized on the Basis of Nanoscale Kirkendall Effect and their Magnetic and Electrochemical Properties. *CrystEngComm*. **2010**, *12*, 1899–1904.
(155) Geller, S. Refinement of the Crystal Structure of Co_9S_8. *Acta Crystallogr*. **1962**, *15*, 1195–1198.
(156) Jin, R.; Liu, J.; Xu, Y.; Li G.; Chen, G. Solvothermal Synthesis and Excellent Electrochemical Performance of Polycrystalline Rose-Like Co_9S_8 Hierarchical Architectures. *J. Mater. Chem. A*. **2013**, *1*, 7995–7999.
(157) Benavente, E.; Santa Ana, M. A.; Mendiźabal F.; Gonźalez, G. Intercalation Chemistry of Molybdenum Disulfide. *Coord. Chem. Rev*. **2002**, *224*, 87–109.
(158) Schonfeld, B.; Huang J. J.; Moss, S. C. Anisotropic Mean-Square Displacements (MSD) in Single-Crystals of 2H-and 3R-MoS_2. *Acta Crystallogr. Sect. B: Struct. Sci*. **1983**, *39*, 404–407.
(159) Py, M. A.; Haering, R. R. Structural Destabilization Induced by Lithium Intercalation in MoS_2 and Related Compounds. *Can. J. Phys*. **1983**, *61*, 76–84.
(160) Gou, X. L.; Chen J.; Shen, P. W. Synthesis, Characterization and Application of SnS_x (x= 1, 2) Nanoparticles. *Mater. Chem. Phys*. **2005**, *93*, 557–566.
(161) Burton, L. A.; Colombara, D.; Abellon, R. D.; Grozema, F. C.; Peter, L. M.; Savenije, T. J.; Dennler G.; Walsh, A. Synthesis, Characterization, and Electronic Structure of Single-Crystal SnS, Sn_2S_3, and SnS_2. *Chem. Mater*. **2013**, *25*, 4908–4916.
(162) Miller, J. B.; Alfonso, D. R.; Howard, B. H.; O'Brien, C. P.; Morreale, B. D. Hydrogen Dissociation on Pd_4S Surfaces. *J. Phys. Chem. C*, **2009**, *113*, 1800-1886.
(163) Gronvold, F.; Rost, E. The Crystal Structures of Pd_4Se and Pd_4S. *Acta Cryst* **1962**, *15*, 11-13.
(164) Vojvodic, A.; Hellman, A.; Ruberto C.; Lindquist, B. I. From Electronic Structure to Catalytic Activity: A Single Descriptor for Adsorption and Reactivity on Transition-Metal Carbides, *Phys. Rev. Lett*. **2009**, *103*, 146103.
(165) Jacobsen, C. J. H.; Dahl, S.; Clausen, B. S.; Bahn, S.; Logadottir A.; Norskov, J. K. Catalyst Design by Interpolation in the Periodic Table: Bimetallic Ammonia Synthesis Catalysts. *J. Am. Chem. Soc*. **2001**, *123*, 8404–8405.
(166) Fujii, H.; Ho jkabe, T.; Kamigaichi, T.; Okamoto, T. Magnetic Properties of Fe_2P Single Crystal. *J. Phys. Soc. Jpn*. **1977**, *43*, 41–46.
(167) Li, H.; Tsai, C.; Koh, A. L.; Cai, L.; Contryman, A. W.; Fragapane, A. H.; Zhao, J.; Han, H. S.; Manoharan, H. C.; AbildPedersen, F.; Norskov, J. K.; Zheng, X, Activating and Optimizing MoS_2

Basal Planes for Hydrogen Evolution through the Formation of Strained Sulphur Vacancies. *Nat. Mater*. **2016**, *15*, 48−53.
(168) Rouxel, J. Anion-Cation Redox Competition and the Formation of New Compounds in Highly Covalent Systems. *Chem. Eur. J.* **1996**, *2*, 1053−1059.
(169) Zhou, Y.; Song, E.; Zhou, J. Auto-optimizing Hydrogen Evolution Catalytic Activity of ReS_2 through Intrinsic Charge Engineering. *ACS Nano.* **2018**, *12*, 4486−4493.
(170) Albani, D.; Shahrokhi, M.; Chen, Z.; Mitchell, S.; Hauert, R.; López, N.; Pérez-Ramírez, J. Selective Ensembles in Supported Palladium Sulfide Nanoparticles for Alkyne Semi-Hydrogenation. *Nat. Commun.* **2018**, *9*, 2634.
(171) Liu, H.; He, Q.; Jiang, H.; Lin, Y.; Zhang, Y.; Habib, M.; Chen, S.; Song, L. Electronic Structure Reconfiguration toward Pyrite NiS_2 via Engineered Heteroatom Defect Boosting Overall Water Splitting. *ACS Nano*. **2017**, *11*, 11574–11583.
(172) Subbaraman, R.; Tripkovic, D.; Chang, K.-C.; Strmcnik, D.; Paulikas, A. P.; Hirunsit, P.; Chan, M.; Greeley, J.; Stamenkovic, V.; Markovic, N. M. Trends in Activity for the Water Electrolyser Reactions on 3d M(Ni,Co,Fe,Mn) Hydr(oxy)oxide Catalysts, *Nat. Mater.* **2012**, *11*, 550−557.
(173) Wagenhofer, M.; Shi, H.; Gutiérrez, O.; Jentys, A.;Lercher J. Enhancing Hydrogenation Activity of Ni-Mo Sulfide Hydrodesulfurization Catalysts, *Sci. Adv.* **2020***, 6*, 5331.
(174) Hein, J.; Hrabar, A.; Jentys, A.; Gutirrez, O. Y.; Lercher, J. A. Al_2O_3-Supported and Unsupported (Ni)MoS_2 for the Hydrodenitrogenation of Quinoline in the Presence of Dibenzothiophene, *ChemCatChem*, **2014**, *6*, 485-499.
(175) León, J.; Kumar, C.; Antúnez-García, J.; Fuentes-Moyado, S. Recent Insights in Transition Metal Sulfide Hydrodesulfurization Catalysts for the Production of Ultra Low Sulfur Diesel: A Short Review, *Catalysts,* **2019***, 9*, 87.
(176) Topsoe, H. The Role of Co–Mo–S Type Structures in Hydrotreating Catalysts. *Appl. Catal. A Gen.* **2007**, *322*, 3–8.
(177) Shimada, H. Morphology and Orientation of MoS_2 Clusters on Al_2O_3 and TiO_2 Supports and their Effect on Catalytic Performance. *Catal. Today* **2003***, 86*, 17–29.
(178) Bara, C.; Lamic-Humblot, A. F.; Fonda, E.; Gay, A. S.; Taleb, A. E.; Devers, E.; Digne, M.; Pirngruber, G. D.; Carrier, X. Surface-Dependent Sulfidation and Rientation of MoS_2 Slabs on Alumina-Supported Model Hydrodesulfurization Catalysts. *J. Catal.* **2016**, *344*, 591–605.
(179) Boullosa-Eiras, S.; Lødeng, R.; Bergem, H.; Stocker, M.; Hannevold L.; Blekkan, E. A. Potential for Metal-Carbide, -Nitride, and -Phosphide as Future Hydrotreating (HT) Catalysts for Processing of Bio-oils. *Catalysis*, **2014**, *26*, 29–71.
(180) Hägg, G. Z. Regularity in the Crystal Structures of Hydrides, Borides, Carbides and Nitrides of the Transition Elements, *Phys. Chem.* **1931**, *12*, 33.
(181) Caputo, R.; Guzzetta, F.; Angerhofer, A. Room-Temperature Synthesis of Nickel Borides via Decomposition of $NaBH_4$ Promoted by Nickel Bromide. *Inorg. Chem.* **2010**, *49*, 8756.
(182) Zhao, E.; Meng, J.; Ma, Y.; Wu, Z. Phase Stability and Mechanical Properties of Tungsten Borides from First Principles Calculations. *Phys. Chem. Chem. Phys*. **2010**, *12*, 13158–13165.
(183) Wang, J.; Ye, T. N.; Gong, Y.; Wu, J.; Miao, N.; Tada, T.; Hosono, H. Discovery of Hexagonal Ternary Phase Ti_2InB_2 and its Evolution to Layered Boride TiB. *Nat. Commun*. **2019**, *10,* 2284.
(184) Gabani S. et al. Magnetism and Superconductivity of Rare Earth Borides, *J. Alloys and Compounds.* **2020**, *821*, 15320.
(185) Greenwood, N.; Parish, R.; Thornton, P. Metal Borides. *Q. Rev., Chem. Soc*. **1965**, *441*.
(186) Xiao, B.; Xing, J. D.; Ding, S. F.; Su, W. Stability, Electronic and Mechanical Properties of Fe_2B. *Phys. B*. **2008**, *403*, 1723.

(187) Zhou, C. T.; Xing, J. D.; Xiao, B.; Feng, J.; Xie, X. J.; Chen, Y. H. First Principles Study on the Structural Properties and Electronic Structure of X_2B (X= Cr, Mn, Fe, Co, Ni, Mo and W) Compounds. *Comput. Mater. Sci*. **2009**, *44*, 1056.

(188) Friedman, R. M.; Hudis, J.; Perlman, M. L.; Watson, R. E. Electronic Behavior in Alloys: Au-Sn. *Phys. Rev. B.* **1973**, *8*, 2433.

(189) Gelatt, C. D. J.; Ehrenreich, H. Charge Transfer in Alloys: AgAu. *Phys. Rev. B*. **1974**, *10*, 398.

(190) Zhang, M.; Wang, H.; Ma, Y. Structural Modifications and Mechanical Properties of Molybdenum Borides from First Principles. *J. Phys. Chem. C.* **2010**, *114*, 6722.

(191) Lawson, J. W.; Bauschlicher, C. W.; Daw, M. S. Ab Initio Computations of Electronic, Mechanical, and Thermal Properties of ZrB_2 and HfB_2. J. *Am. Ceram. Soc*. **2011**, *94*, 3494.

(192) Furimsky, E. Metal Carbides and Nitrides as Potential Catalysts for Hydroprocessing. *Appl. Catal., A,* **2003**, *240*, 1–28.

(193) Oyama, S. T. Preparation and Catalytic Properties of Transition Metal Carbides and Nitrides. *Catal. Today*. **1992**, *15*, 179.

(194) Demczyk, B. G.; Choi J. G. Thompson, L. T. Surface Structure and Composition of High-Surface-Area Molybdenum Nitrides. *Appl. Surf. Sci*. **1994**, *78*, 63–69.

(195) Chen, Y. D.; Li, C.; Zhou, J.; Zhang, S.; Rao, D.; He, S.; Wei, M.; Evans, D. G.; Duan, X. Metal Phosphides Derived from Hydrotalcite Precursors toward the Selective Hydrogenation of Phenylacetylene. *ACS Catal*. **2015**, *5*, 5756-5765.

(196) Paul, R.; Buisson P.; Josesph, N. Catalytic Activity of Nickel Borides. *Ind. Eng. Chem*. **1952**, *44*, 1006–1010.

(197) Li, H. X.; Li, H.; Dai W.; Qiao, M. Preparation of the Ni-B Amorphous Alloys with Variable Boron Content and its Correlation to the Hydrogenation Activity. *Appl. Catal., A*. **2003**, *238*, 119–130.

(198) Acosta, D.; Ramirez, N.; Erdman, E.; Destefanis H.; Gonzo, E. Transition Metals as Dopants on Nickel Borides: Their Catalytic Activity Effect on Hydrogenation Reactions. *Catal. Today*. **2008**, *133–135*, 49–55.

(199) Nozaki F.; Adachi, R. Chemical Composition of the Catalyst Prepared by Reduction of Nickel Orthophosphate in Hydrogen and Catalytic Activity for Partial Hydrogenation of 1, 3-Butadiene. *J. Catal*. **1975**, 40, 166–172.

(200) Nozaki, F.; Kitoh T.; Sodesawa, T. Promoting Effect of Oxygen for Hydrogenation of Butadiene over Ni_2P Catalyst. *J. Catal*. **1980**, *62*, 286–293.

(201) Shi, C.; Hoisington, R.; Jang, B. Promotion Effects of Air and H_2 Nonthermal Plasmas on TiO_2 Supported Pd and Pd-Ag Catalysts for Selective Hydrogenation of Acetylene, *Ind. Eng. Chem. Res.* **2007***, 46*, 4390-4395.

(202) McCue, A. J.; Guerrero-Ruiz, A.; Ramirez-Barria, C.; Rodríguez-Ramos, I.; Anderson, J. A. Selective Hydrogenation of Mixed Alkyne/Alkene Streams at Elevated Pressure over a Palladium Sulfide Catalyst. *J. Catal*. **2017**, *355*, 40–52.

(203) McCue, A. J.; Guerrero-Ruiz, A.; Rodríguez-Ramos, I.; Anderson, J. A. Palladium Sulphide-A Highly Selective Catalyst for the Gas Phase Hydrogenation of Alkynes to Alkenes. *J. Catal*. **2016**, *340*, 10–16.

(204) Liu, Y. N.; Li, Y. W.; Anderson, J. A.; Feng, J. T.; Guerrero-Ruiz, A.; Rodríguez-Ramos, I.; McCue, A. J.; Li, D. Q. Comparison of Pd and Pd_4S based Catalysts for Partial Hydrogenation of External and Internal Butynes. *J. Catal*. **2020**, *383*, 51–59.

(205) Carenco, S.; Leyva-Pérez, A.; Concepcion, P.; Boissière, C.; Mézailles, N.; Sanchez, C.; Corma, A. Nickel Phosphide Nanocatalysts for the Chemoselective Hydrogenation of Alkynes. *Nano Today*. **2012**, *7*, 21–28.
(206) Zhao, M. Fabrication of Ultrafine Palladium Phosphide Nanoparticles as Highly Active Catalyst for Chemoselective Hydrogenation of Alkynes. *Chem. Asian J*. **2016**, *11*, 461-464.
(207) Belykh, L. B.; Skripov. N. I.; Sterenchuk. T. P.; Gvozdovskay, K. L.; Sanzhieva, S. B.; Schmidt, F. K. Pd-P Nanoparticles as Active Catalyst for the Hydrogenation of Acetylenic Compounds. *J. Nanopart Res*. ***2019***, *21*, 198.
(208) Skripov, N. I.; Belykh, L. B.; Sterenchuk, T. P.; Gvozdovskaya, K. L.; Zherdev, V. V.; Dashabylova, T. M.; Schmidt F. K. Palladium-Phosphorus Nanoparticles as Effective Catalysts of the Chemoselective Hydrogenation of Alkynols, *Kinetics and Catalysis*, **2020**, *61*, 575–588.
(209) Zhao, M.; Ji, Y.; Wang, M.; Zhong, N.; Kang, Z.; Asao, N.; Jiang, W. Composition-Dependent Morphology of Bi- and Trimetallic Phosphides: Construction of Amorphous Pd−Cu−Ni−P Nanoparticles as a Selective and Versatile Catalyst. *ACS Appl. Mater. Interfaces*. **2017**, *9*, 34804−34811.
(210) Albani, D.; Shahrokhi, M.; Chen, Z.; Mitchell, S.; Hauert, R.; López, N.; Pérez Ramírez, J. Selective Ensembles in Supported Palladium Sulfide Nanoparticles for Alkyne Semi-Hydrogenation. *Nat. Commun*. **2018**, *9*, 2364.
(211) Liu, P.; Rodriguez, J. A.; Asakura, T.; Gomes J.; Nakamura, K. Desulfurization Reactions on Ni_2P(001) and α-Mo_2C(001) Surfaces: Complex Role of P and C Sites. *J. Phys. Chem. B*. **2005**, *109*, 4575–4583.
(212) Zhou, S.; Chen, J.; Liu, X.; Zhang, J. Influence of Reduction Conditions on the Catalytic Activity of Ni_2P/SiO_2 for Gas-Phase Hydrodechlorination of Chlorobenzene. *Chin. J. Catal*. **2007**, *28*, 498.
(213) Liu, X.; Chen, J.; Zhang, J. Hydrodechlorination of Chlorobenzene over Silica-Supported Nickel Phosphide Catalysts. *Ind. Eng. Chem. Res*. **2008**, *47*, 5362.
(214) Wu, Z.; Sun, F.; Wu, W.; Feng, Z.; Liang, C.; Wei, Z.; Li, C. On the Surface Sites of MoP/SiO_2 Catalyst under Sulfiding Conditions: IR Spectroscopy and Catalytic Reactivity Studies. *J. Catal.,* **2004**, *222*, 41–52.
(215) Y. K. Lee, S. T. Oyama, Bifunctional Nature of a SiO_2-Supported Ni_2P Catalyst for Hydrotreating: EXAFS and FTIR Studies, *J. Catal.* **2006**, *239*, 376–389.
(216) Ding, L. N.; Wang, A. Q.; Zheng, M. Y.; Zhang, T. Selective Transformation of Cellulose into Sorbitol by Using a Bifunctional Nickel Phosphide Catalyst, *ChemSusChem* **2010**, *3*, 818–821.
(217) Yang, P.; Kobayashi, H.; Hara, K.; Fukuoka, A. Phase Change of Nickel Phosphide Catalysts in the Conversion of Cellulose into Sorbitol, *ChemSusChem* **2012**, *5*, 920–926.
(218) Oyama, S. T. Production of Phenol and Cresol from Guaiacol on Nickel Phosphide Catalysts Supported on Acidic Supports, *Top Catal*. **2015**, *58*, 201–210.
(219) Lan, X.; Pestman, R.; Hensen, E. J. M.; Weber, T. Furfural Hydrodeoxygenation (HDO) over Silica-Supported Metal Phosphides the Influence of Metal-Phosphorus Stoichiometry on Catalytic Properties, *J. Catal.* **2021,** DOI: 10.1016/j.jcat.2021.01.031
(220) Golubeva, M. A.; Maximov A. L. Hydroprocessing of Furfural over In Situ Generated Nickel Phosphide based Catalysts in Different Solvents, *Appl. Catal. A, Gen.* **2020**, *608*, 117890.
(221) Li, X.; Zhang, Y.; Wang, A.; Wang, Y.; Hu, Y. Influence of TiO_2 and CeO_2 on the Hydrogenation Activity of Bulk Ni_2P. *Catal. Commun*. **2010**, *11(14)*, 1129-1132.
(222) Gao, R.; Pan, L.; Wang, H.; Zhang, X.; Wang, L.; Zou, J. Ultradispersed Nickel Phosphide on Phosphorus-Doped Carbon with Tailored D-band Center for Efficient and Chemoselective Hydrogenation of Nitroarenes. *ACS Catal.* **2018**, *8*, 8420−8429.
(223) Wei, L.; Liu, D. J.; Rosales, B. A.; Evans, J. W.; Vela, J. Mild and Selective Hydrogenation of Nitrate to Ammonia in the Absence of Noble Metals. *ACS Catal*. **2020**, *10 (6*), 3618–3628.

(224) Furukawa, S.; Matsunami, Y.; Hamada, I.; Hashimoto, Y.; Sato, Y.; Komatsu, T. Remarkable Enhancement in Hydrogenation Ability by Phosphidation of Ruthenium: Specific Surface Structure Having Unique Ru Ensembles. *ACS Catal*. **2018**, *8 (9)*, 8177–8181.
(225) Ma, R.; Yang, T.; Gao, J.; Kou, J.; Zhu Chen, J.; He, Y.; Miller, J. T.; Li, D. Composition Tuning of Ru-Based Phosphide for Enhanced Propane Selective Dehydrogenation. *ACS Catal.* **2020**, *10*, 10243−10252.
(226) Rostrup-Nielsen, J. R. Catalytic Steam Reforming. Catalysis (Science and Technology), **1984**, 5, 1-117.
(227) Pei, Y.; Guo, P.; Qiao, M.; Li, H.; Wei, S.; He H.; Fan, K. The Modification Effect of Fe on Amorphous CoB Alloy Catalyst for Chemoselective Hydrogenation of Crotonaldehyde. *J. Catal*. **2007**, *248*, 303–310.
(228) Liang, Y.; Liu, Q.; Asiri, A. M.; Sun, X.; Luo, Y. Self-Supported FeP Nanorod Arrays: A Cost-Effective 3D Hydrogen Evolution Cathode with High Catalytic Activity, *ACS Catal*. **2014**, *4*, 4065−4069.
(229) Yu S. H.; Chua, D. H. C. Toward High-Performance and Low-Cost Hydrogen Evolution Reaction Electrocatalysts: Nanostructuring Cobalt Phosphide (CoP) Particles on Carbon Fiber Paper, *ACS Appl. Mater. Interfaces*. **2018**, *10*, 14777–14785.
(230) Xu, Y. F.; Duchesne, P. N.; Wang, L.; Tavasoli, A.; Jelle, A. A.; Xia, M.; Liao, J. F.; Kuang, D. B.; Ozin, G. A. High-Performance Light-Driven Heterogeneous CO_2 Catalysis with Near-Unity Selectivity on Metal Phosphides. *Nat. Commun*. **2020**, *11*, 5149.
(231) Guan, B. Y.; Yu, L.; Wang, X.; Song S.; Lou, X. W. Formation of Onion-Like $NiCo_2S_4$ Particles via Sequential Ion-Exchange for Hybrid Supercapacitors, *Adv. Mater*. **2017**, *29*, 1605051.
(232) Liu, Y.; Fang, Y.; Zhao, Z.; Yuan C.; Lou, X. W. A Ternary $Fe_{1-x}S$@Porous Carbon Nanowires/Reduced Graphene Oxide Hybrid Film Electrode with Superior Volumetric and Gravimetric Capacities for Flexible Sodium Ion Batteries, *Adv. Energy Mater*. **2019**, *9*, 1803052.
(233) Park, H.; Kwon, J.; Choi, H.; Shin, D.; Song T.; X. Lou, W. D. Unusual Na^+ Ion Intercalation/Deintercalation in Metal-Rich $Cu_{1.8}S$ for Na-Ion Batteries, *ACS Nano*. **2018**, *12*, 2827–2837.
(234) Geng, P.; Zheng, S.; Tang, H.; Zhu, R.; Zhang, L.; Cao, S.; Xue H.; Pang, H. Transition Metal Sulfides Based on Graphene for Electrochemical Energy Storage, *Adv. Energy Mater*. **2018**, *8*, 1703259.
(235) Wang, S.; Fang, Y.; Wang X.; Lou, X. W. Hierarchical Microboxes Constructed by SnS Nanoplates Coated with Nitrogen-Doped Carbon for Efficient Sodium Storage, *Angew. Chem., Int. Ed*. **2019**, *131*, 770–773.
(236) Wang, J.; Lin, S.; Tian, N.; Ma, T.; Zhang, Y.; Huang, H. Nanostructured Metal Sulfides: Classification, Modification Strategy, and Solar-Driven CO_2 Reduction Application. *Adv. Funct. Mater.* **2020**, 2008008.
(237) Sarilmaz, A.; Yanalak, G.; Aslan, E.; Ozel, F.; Patir, I. H.; Ersoz, M. Shape-controlled synthesis of copper based multinary sulfide catalysts for enhanced photocatalytic hydrogen evolution, *Renewable Energy,* **2021**, *164*, 254-259.

For Table of Contents Only